Title

Optical Properties of Wintertime Aerosols from Residential Wood Burning in Fresno, CA: Results from DISCOVER-AQ 2013

Authors

Zhang, Xiaolu
Kim, Hwajin
Parworth, Caroline L
et al.

Publication Date

2016

Peer reviewed

Optical Properties of Wintertime Aerosols from Residential Wood Burning in Fresno, CA: Results from DISCOVER-AQ 2013

Xiaolu Zhang[1], Hwajin Kim[2,3], Caroline Parworth[2], Dominique Young[2], Qi Zhang[2], Andrew R. Metcalf[4], Christopher D. Cappa[1,*]

[1]Department of Civil and Environmental Engineering, University of California, Davis, CA 95616

[2]Department of Environmental Toxicology, University of California, Davis, CA 95616

[3] Now at: Center for Environment, Health and Welfare Research, Korea Institute of Science and Technology, Seoul 136-701, Republic of Korea

[4]Department of Mechanical Engineering, University of Minnesota, Minneapolis, MN 55455

[*] Corresponding author

Email: cdcappa@ucdavis.edu

Phone: (530) 752-8180

Address: Department of Civil and Environmental Engineering, 3135 Ghausi Hall, University of California, One Shields Avenue, Davis, CA 95616

Key words: DISCOVER-AQ, $PM_{2.5}$, optical properties, absorption enhancement, brown carbon, refractive index

Abstract

The optical properties, composition and sources of the wintertime aerosols in the San Joaquin Valley (SJV) were characterized through measurements made in Fresno, CA during the 2013 DISCOVER-AQ campaign. $PM_{2.5}$ extinction and absorption coefficients were measured at 405, 532 and 870 nm along with refractory black carbon (rBC) size distributions and concentrations. BC absorption enhancements (E_{abs}) were measured using two methods, a thermodenuder and mass absorption coefficient method, which agreed well. Relatively large diurnal variations in the E_{abs} at 405 nm were observed, likely reflecting substantial nighttime emissions of wood burning organic aerosols (OA) from local residential heating. Comparably small diurnal variations and absolute nighttime values of E_{abs} were observed at the other wavelengths, suggesting limited lensing-driven enhancement. Positive matrix factorization analysis of OA mass spectra from an aerosol mass spectrometer resolved two types of biomass burning OA, which appeared to have different chemical composition and absorptivity. Brown carbon (BrC) absorption was estimated to contribute up to 30% to the total absorption at 405 nm at night but was negligible (<10%) during the day. Quantitative understanding of retrieved BrC optical properties could be improved with more explicit knowledge of the BC mixing state and the distribution of coating thicknesses.

1. Introduction

Recent studies in the past decade or so have suggested a substantial positive radiative forcing (i.e. global warming effect) of atmospheric black carbon (BC).[1-3] The most recent scientific assessment estimated BC to be the second largest anthropogenic warming agent, with its direct radiative forcing (DRF) estimated to be 0.71 ± 0.17 W m^{-2}.[1] However, uncertainties in the forcing remain due to limitations in knowledge of the emission, spatial distribution, [2] mixing state,[3] and contribution from non-BC species to observed absorption.[1]

The observable light absorption coefficient for BC, $b_{abs,BC}$, depends on particle mixing state.[4-5] The magnitude of $b_{abs,BC}$ can be enhanced by internal mixing of non-absorbing "coating" materials with BC (sometimes colloquially referred to as the "lensing" effect and here referred to as the mixing effect).[4,6] BC is often co-emitted and mixed with organic compounds, some of which absorb and in which case are collectively referred to as brown carbon (BrC).[7] The specific properties of BrC vary with source and production mechanism,[8-12] yet remain incompletely characterized. The quantification and attribution of the total observable b_{abs} to these different effects and components is critical for accurately estimating the absorption aerosol optical depth (AAOD) and direct radiative forcing (DRF) caused by each aerosol component.

Laboratory studies[13-15] and theoretical calculations[5,16] suggest substantial mixing-related absorption enhancement is possible for typical atmospheric particles, leading some to apply an *ad hoc* factor of 1.5 upward scaling of simulated BC AAOD in models.[1] This scaling, together with the inclusion of BrC, has been shown to reduce, although not eliminate, the model low bias compared to remotely sensed AAOD, a primary constraint for BC DRF.[17] However, recent observations of the absorption enhancement (E_{abs}) for particles undergoing

photochemical aging near urban centers indicated that E_{abs} from mixing can be smaller than expected, even for thickly coated BC particles,[18] although the extent to which this is true around the world and in all environments remains unclear.[19-21] Additionally, the separation of the BC AAOD from the total observed AAOD is subject to considerable uncertainty.[1] The lack of constraints on the apportioned b_{abs} components in both modeled and observed AAOD contributes substantially to uncertainty in the BC DRF (along with emissions and vertical distributions).

One approach to apportion b_{abs} into contributions from BC ($b_{abs,BC}$), mixing ($b_{abs,mixing}$) and BrC ($b_{abs,BrC}$) utilizes the different wavelength (λ) dependencies (i.e., absorption Angström exponents, AAE) of BC and BrC. $b_{abs,BC}$ is typically assumed to vary inversely with λ (AAE of ~ 1), whereas $b_{abs,BrC}$ typically exhibits a stronger λ dependence (AAE > 1) and is assumed to absorb negligibly at longer wavelengths (λ > ~600 nm).[9,22-23] The AAE method is the basis for apportioning remotely sensed AAOD to different absorbing components.[24-25] However, the method cannot characterize the influence of mixing and is confounded by knowledge of the exact AAE for BC,[26] making it only a robust estimation under limited circumstances, i.e. AAE > 1.6.[16] A second approach compares measured mass absorption coefficients (MAC) for atmospheric BC to a reference state (e.g., fresh emitted nascent BC)[27]. The use of absolute MAC values requires accurate measurements of both BC mass concentrations and absorption coefficients, as well as consistency of the operational definitions among the measurements. Unrealistically low or high MAC values have often been found, possibly as a result of inaccurate or inconsistent measurements. A third approach characterizes b_{abs} before and after *in situ* heating in a thermodenuder (TD) to remove BC coatings and externally-mixed BrC.[18,21,28-30] The TD method is independent of instrument calibration or inter-comparison,

but complete removal of the coating materials is critical and may not always occur. Ideally, combinations of the above approaches can be used to overcome the complications associated with any individual methodology.

The San Joaquin Valley (SJV) in central California has suffered from severe air pollution problems for decades.[31-32] Previous studies focused on this region have shown that primary emissions, such as vehicles, cooking, residential wood combustion, and agricultural activities,[33-37] are the major sources of particulate matter (PM) during winter. However, few studies have characterized optical properties of the wintertime aerosol. In this work, highly time resolved *in situ* measurements of $PM_{2.5}$ light extinction and absorption made in conjunction with a broad suite of aerosol chemical composition measurements during the DISCOVER-AQ 2013 campaign in Fresno, CA are reported on. The particularly cold and dry winter of 2013 led to high PM concentrations,[38] with major contributions from residential wood burning emissions. The diurnal and episodic variability of the optical properties and their connection with the chemical composition and emissions sources are quantitatively examined to investigate the sources and climate effect of the light-absorbing particles. The key optical properties of residential burning aerosols are calculated and implications for aerosol DRF and emissions control in the SJV and the state of California are discussed.

2. Experimental Method

2.1 Sampling

During the NASA DISCOVER-AQ 2013 California campaign, a suite of ground measurements of $PM_{2.5}$ chemical composition and optical properties were carried out from January 13 to February 11, 2013 at the California Air Resources Board (CARB) Fresno-Garland air monitoring facility (36.7854°, -119.7732°). The site is surrounded by residential

and commercial areas and is approximately 1500 m to the east of Yosemite FWY-41. Particles were sampled into the building from 1.5 m above the rooftop through 4 m of 1/2 in. diameter stainless steel tubing. The air stream passed through a $PM_{2.5}$ cyclone (URG) at 16.7 lpm and distributed to the various instruments through 1/4 in. or 3/8 in. tubing.

2.2 Instrumentation

Table S1 summarizes the instruments and measurements made at the Fresno ground site. $PM_{2.5}$ light extinction (b_{ext}) and absorption (b_{abs}) coefficients at 405 and 532 nm were measured for dried particles (relative humidity < 30%) with the UC Davis cavity-ringdown photoacoustic spectrometer (CRD-PAS).[39-41] The PAS was calibrated approximately every five days using gas-phase O_3 by referencing the observed photoacoustic signal to the corresponding b_{ext} measured by the CRD.[39] $PM_{2.5}$ b_{ext} and b_{abs} values were also measured at 870 nm with a PhotoAcoustic eXtinctiometer (PAX; DMT, Boulder, CO, USA). The PAX was calibrated prior to and after the campaign using atomized Aquadag and PSL particles for the absorption and scattering channel, respectively. Instrument zeros were determined using filtered ambient air for 3 min of every 30 min. The 1σ standard deviations in b_{abs} for filtered air at the 2 s sampling time were measured to be approximately 0.8 Mm^{-1} (405 nm), 0.4 Mm^{-1} (532 nm), and < 1 Mm^{-1} (870 nm). The uncertainties in b_{ext} were estimated to be 5% (405 nm, 532 nm and 870 nm) and in b_{abs} were 10% at 532 nm and 20% at 405 nm and 870 nm.

Refractory black carbon (rBC) mass concentrations and size distribution measurements were made with a DMT Single Particle Soot Photometer (SP2),[42] which was calibrated with atomized and size-selected Fullerene soot particles before and after the campaign. Fullerene soot has been shown to provide a similar response in the SP2 per unit mass as diesel and biomass burning derived rBC.[43] The masses of individual rBC particles were measured from

which rBC volume equivalent diameters (d_{ve}) were calculated assuming this mass is compacted to a spherical particle with a density of 1.8 g cm^{-3}.[44] The observed 5-min average rBC volume-weighted size distributions (from 100 nm ≤ d_{ve} ≤ 300 nm) were individually fit using a bimodal lognormal distribution. The fits were extrapolated to 20-1000 nm to estimate the "missing" rBC mass outside the measurement range. The overall shape of the rBC size distribution and mode diameter varied throughout the day, indicating variations in the dominant rBC source (vehicles versus wood combustion; Fig. S1a). Consequently, a unique "missing" mass correction was applied for each 5 min period, as opposed to a single campaign-average value. Here, we assume that the "missing" portion follows the same bimodal lognormal distributions as those directly observed. The SP2 rBC concentrations were compared with daily-average elemental carbon (EC) measurements made every 3rd day by CARB. The measured [rBC] was ~30% lower than the [EC], which could indicate a systematic bias in the SP2 (due, perhaps, to deviations in the assumed shape in the missing-mass regions or calibration errors) or in the EC measurements (Fig. S2). The 1σ standard deviation in the rBC mass, characterized during a period when the rBC concentration was relatively stable, is 0.06 μg m^{-3}. The uncertainty in rBC mass is estimated to be at least 50%, considering the uncertainties associated with the instrument operation, external calibration, and the lognormal fits. Further discussion is provided in Section 3.2.

The mass concentrations of submicron (PM_1) non-refractory (NR) inorganic (NH_4^+, SO_4^{2-}, NO_3^-, Cl^-) and organic aerosols (OA) were determined with an Aerodyne High Resolution Time-of-Flight Aerosol Mass Spectrometer (HR-ToF-AMS).[45] Positive Matrix Factorization (PMF) analysis was performed on the OA mass spectral matrix[46] and six OA components were resolved: two types of biomass burning OA (BBOA-1 and BBOA-2), hydrocarbon-like

OA (HOA), semi-volatile oxygenated OA (SV-OOA), low volatility oxygenated OA (LV-OOA), cooking OA (COA). The sum of the two BBOA factors will be referred to as BBOA. *Young et al.*[38] provide detailed information about the HR-ToF-AMS operation and data analysis. Hourly meteorological data (e.g., ambient temperature, relative humidity) and trace gases (e.g., NO_x, CO, SO_2) were routinely measured at the CARB Fresno-Garland monitoring site.

Particle size distributions over the diameter range of 16-685 nm mobility diameter (d_m) were measured with a Scanning Mobility Particle Sizer (SMPS; TSI, Inc.). Particle size distributions from 0.8-2.5 μm aerodynamic diameter (d_a) were determined with an Aerodynamic Particle Sizer (APS; TSI, Inc.). A merged ambient particle size distribution (Fig. S3) was determined from the SMPS and APS distributions after adjusting the APS d_a values to mobility-equivalent values (d_m) using time-dependent particle density values and slip correction factor. The particle density was estimated by comparison of the PM_1 volume concentrations calculated from the size distribution and the AMS-measured bulk PM_1 mass concentrations.

2.3 Thermodenuder

The CRD-PAS, PAX, SP2 and SMPS alternatively sampled either ambient particles or particles that passed through a thermodenuder on an automated 5 min cycle. The TD was a 1 in. OD, 36 in. long stainless steel tube with the first 18 in. heated to 175 °C and the second 18 in. to 275 °C. The final 12 in. contained an activated charcoal cloth held around the inner circumference with rolled stainless steel mesh. The residence time in the dual-heating stage of the TD was ~7 s at room temperature. The two-stage heating was utilized to help minimize charring of the sample particles. Ambient (bypass) sampling was done through an unheated

stainless steel tube of the same dimensions as the TD. All TD data were corrected for particle losses relative to the bypass using a transmission factor of 0.88, determined from measurements of size-selected Fullerene soot particles.

2.4 Absorption Enhancement

Two independent methods were used to characterize and quantify the absorption enhancement (E_{abs}) that results from the (time-varying) combination of internal mixing of rBC particles and BrC absorption. In the first (the TD method), E_{abs} is the ratio between ambient particle ($b_{abs,ambient}$) and TD particle ($b_{abs,TD}$) absorption:[18,21]

$$E_{abs,TD} = \frac{b_{abs,ambient}}{b_{abs,TD}} \quad (1)$$

Heating in the TD induces evaporation of non-refractory PM and leaves behind, ideally, pure rBC particles.

In the second method, E_{abs} was determined from measurements of the mass absorption coefficient (MAC), defined as $MAC = b_{abs,ambient}/m_{rBC}$, where m_{rBC} is the rBC mass concentration. $E_{abs,MAC}$ can be estimated by normalizing the observed MAC by some reference MAC that is characteristic of pure rBC, i.e. $E_{abs,MAC} = MAC_{obs}/MAC_{ref}$. The accuracy of the MAC method to determine $E_{abs,MAC}$ is limited by the accuracy of the b_{abs} and m_{rBC} and by knowledge of MAC_{ref}. For this analysis, wavelength-specific MAC_{ref} values are estimated by forcing good agreement between $E_{abs,MAC}$ and the daily minimum in $E_{abs,TD}$ (see Sect. 3.2 and Fig. 2b). (Alternatively, MAC_{ref} could be taken from the literature. However, as we are primarily interested in variations in the MAC and since the m_{rBC} are somewhat uncertain, we have adopted this alternative approach.) This definition allows for direct comparison of the temporal variation in E_{abs} between the two methods and makes the derived $E_{abs,MAC}$ values, in

197 particular, their temporal variations, dependent upon the instrument precision, rather than
198 accuracy (further discussed in Sect. 3.2).

199 **3. Results and discussion**

200 **3.1 Overview of DISCOVER-AQ Fresno Measurements.**

201 Fig. 1 provides an overview of meteorological conditions (temperature and relative
202 humidity (RH)) and of aerosol optical properties and chemical composition observed during
203 the campaign. The average NR-PM_1 mass concentration was more than two times higher
204 (26.4 μg m^{-3} vs. 11.9 μg m^{-3}) during DISCOVER-AQ than during a previous study in Fresno
205 in winter 2010.[37] The average OA concentration in 2013 was ~1.5 times higher (11.9 μg m^{-3}
206 vs. 7.9 μg m^{-3}), including a ~3 times higher average BBOA concentration (3.6 μg m^{-3} vs. 1.24
207 μg m^{-3}). Two severe air pollution episodes (1/14-1/23 and 1/29-2/5) having $PM_{2.5}$
208 concentrations exceeding the National Ambient Air Quality Standards (NAAQS, 24-hr
209 average of 35 μg m^{-3}) occurred. These two episodes were separated by a relatively clean
210 period (1/24-1/27) that was identified as being marine influenced with enhanced particulate
211 Cl^- and SO_4^{2-} concentrations.[38] The mass extinction coefficient (MEC), which is the ratio
212 between b_{ext} and [PM_1], was slightly larger during the clean period than the polluted periods
213 (Fig. S4). This is consistent with an increased contribution of coarse-mode particles during the
214 clean period compared to the pollution episodes, when the majority of PM mass was in
215 submicrometer particles (D_p < 1μm) (Fig.S5).

216 There is a strong diurnal variation in most of the measured PM properties (Fig. S6). The
217 fraction of BBOA in total PM_1 mass is highest at night, when the temperatures are lowest
218 (T_{amb} often below 0°C), while the fraction of secondary OA components (SV-OOA and LV-
219 OOA) was highest during the daytime (T_{amb} ~ 10-20°C). This leads to a negative correlation

between T_{amb} and the ratio of BBOA:OA throughout the study (Fig. S7), which is relatively insensitive to meteorological conditions (i.e. no major shift in the correlation was observed for polluted vs. clean periods). This strongly suggests that the greater contribution of BBOA during the cold winter of 2013 (relative to 2010)[37] is driven primarily by enhanced emissions from residential wood burning for domestic heating.

The campaign average dry $PM_{2.5}$ b_{ext} and b_{abs} at 532 nm were 130.8 and 13.5 Mm^{-1}, respectively, corresponding to a single scatter albedo (*SSA*) of 0.90. $PM_{2.5}$ $b_{ext,532nm}$ was well correlated with the PM_1 mass concentrations (r^2 = 0.86) (Fig. S4), with an average MEC of 3.76 m^2g^{-1}. The b_{abs} were highly correlated with rBC mass concentration (405 nm: r^2 = 0.95 ; 532 nm: r^2 = 0.95; 870 nm: r^2 = 0.97), although rBC only accounts for < 5% of total PM_1 mass. The b_{abs}, *SSA* and, to a lesser degree, b_{ext} of $PM_{2.5}$ vary diurnally (Fig. S6a). During the day, $b_{abs,532nm}$ was strongly influenced by vehicle emissions, indicated from the peak during morning rush hour that coincides with the peak in HOA (Fig. S6b). At night, $b_{abs,532nm}$ is nearly 5 times higher than daytime while $b_{ext,532nm}$ increases by only a factor of 1.7, leading to a lower nighttime aerosol SSA. The BBOA concentration is also enhanced at night, by a factor of ~5. The clear diurnal variability in chemical composition, driven by variations in the dominating aerosol sources, allows for assessment of the optical properties of aerosol components from different sources.

3.2 Absorption Enhancement

The observed wavelength-dependent b_{abs} and E_{abs} include contributions from rBC, internal mixing of rBC with other NR materials, and absorption by BrC. The campaign average $E_{abs,TD}$ at 405, 532 nm and 870 nm were 1.27±0.17, 1.18±0.06 and 1.21±0.09, respectively. The observed E_{abs} exhibit wavelength-specific diurnal dependencies (Fig. 2). At 405 nm and 532

nm, the E_{abs} during nighttime are larger than during daytime, especially at 405 nm, whereas at 870 nm, the E_{abs} is slightly larger during daytime. The $E_{abs,TD}$ and $E_{abs,MAC}$ are relatively similar in magnitude, although the $E_{abs,MAC}$ exhibit a somewhat larger diurnal variation than do the $E_{abs,TD}$. (Recall that MAC_{ref} has been defined here to ensure good agreement with the daily minimum $E_{abs,TD}$.) The similar magnitudes and distributions of the observed E_{abs} at 532 and 870 nm suggest that 1) non-BC particles do not absorb significantly at $\lambda > \sim 500$ nm, and 2) internal mixing of BC with other NR-PM contributes only moderately (~10-20%) to the enhancement of the BC absorption. The limited enhancement observed here is likely due to either limited amounts of coating material existing on the BC or the particles having an internal morphology that differs from the ideal core-shell configuration.[18] The relatively narrow E_{abs} distributions and small day-night differences at 532 nm and 870 nm suggest that the mean particle mixing (i.e. coating) state, or at least the influence of such coatings on BC absorption, does not strongly differ between the major BC sources (i.e. vehicle emissions vs. fresh residential wood combustion). These observations of relatively small E_{abs} due to internal mixing are similar to previous measurements made in the summertime in other urban environments in California,[18] where relatively thickly-coated particles were observed; in Nagoya, Japan,[30] where the particles tended to be relatively thinly coated; and in Toronto, Canada,[20] where local, wildfire-impacted and transboundary (aged) particles were sampled. They are, however, lower than those reported for air masses dominated by freshly emitted particles from the Four Mile Canyon fire in Colorado ($E_{abs,532nm}$~1.4)[21] and for some air masses sampled in Detling, UK (near London).[19]

The comparatively larger average $E_{abs,405nm}$ during nighttime ($E_{abs,TD}$ ~ 1.4; $E_{abs,MAC}$ ~ 1.5) indicates a strong contribution of BrC to the observed $b_{abs,405nm}$, whereas the similarity of

266 $E_{abs,405nm}$ to the other wavelengths and the relatively small values during the day suggests
267 limited BrC contributions during the day (Fig. 2). There is a good correlation between
268 $E_{abs,405nm}$ and the BBOA-to-OA mass concentration ratio (BBOA:OA; Fig. 3a), which together
269 with the observed diurnal behavior clearly implicates nighttime residential wood burning is an
270 important BrC source in this region. The decrease in $E_{abs,405nm}$ during daytime likely results
271 from ventilation, vertical mixing, or particle evaporation.

272 The two BBOA factors, BBOA-1 and BBOA-2, were identified from the PMF analysis in
273 part based on enhanced signals at ion $C_2H_4O_2^+$ (m/z 60) and $C_3H_5O_2^+$ (m/z 73) in their mass
274 spectra[47-48] (detailed mass spectra information is presented by *Young et al.*[38]). The relative
275 contributions of BBOA-1 and BBOA-2 varied throughout the study, especially between the
276 two PM episodes (Fig. S8a). BBOA-2 has a more pronounced day/night variation compared
277 to BBOA-1 (Fig. S8b). The $E_{abs,405nm}$ exhibited strong, approximately linear relationship with
278 the BBOA-2:OA ratio, but had almost no dependence on the BBOA-1: OA ratio (Fig. 3b and
279 3c). This suggests that BBOA-2 may be more absorbing than BBOA-1. BBOA-2 has a higher
280 O:C ratio and a smaller f_{44} : f_{60} ratio,[38] suggesting that the different absorptivity for BBOA-1
281 and BBOA-2 may be linked to the difference in their chemical compositions. (f_{44} and f_{60} are
282 the fraction of the signal at *m/z* 44 and 60 in the AMS OA mass spectra, respectively). Several
283 laboratory and ambient studies have observed variability in the OA composition and
284 absorptivity under different burning conditions, e.g., combustion temperature, burning load,
285 and fuel type.[21,28,49-50] The seemingly more absorbing BBOA-2 is the dominant BBOA type
286 during the second PM episode when the ambient temperature was higher (Fig. 1), possibly
287 indicating some difference in the typical burn conditions (e.g., burning load/temperature),
288 which can affect BBOA/BC emission ratio.[51]

The $E_{abs,MAC}$ and $E_{abs,TD}$ exhibited similar diurnal peak-to-trough amplitude differences. However, the absolute nighttime average $E_{abs,MAC}$ are slightly larger, and the overall distributions are somewhat wider at all three wavelengths. These relatively minor differences between $E_{abs,TD}$ and $E_{abs,MAC}$ could result from biases or errors in either of the methods. Biases in $E_{abs,TD}$ tend to be negative (i.e. depress E_{abs}) and can potentially result from i) residual BC "coatings" that did not fully evaporate in the TD, ii) residual BrC that did not fully evaporate in the TD, or iii) "browning" of residual OA in the TD. Biases or errors in $E_{abs,MAC}$ result from time-varying biases or errors in the b_{abs} or m_{rBC} measurements, with an underestimate of m_{rBC} leading to an overestimate of MAC, or vice versa. We posit that the biases or errors in the m_{rBC} determined by the SP2 is more likely responsible for the difference between methods in this study because the magnitude of the discrepancy between nighttime $E_{abs,TD}$ and $E_{abs,MAC}$ is similar across all three wavelengths (~10%). The SP2 measurements require correction for rBC outside the detection range and, although this "missing" mass is approximately accounted for through bimodal fitting of SP2 size distributions with high time resolution, the robustness of this correction may vary with time/source. Consider that the MAC_{TD} at all three wavelengths during the daytime are slightly smaller than those during morning and evening rush hours and those around midnight, when the BBOA and rBC concentrations peak (Fig. S9). This could indicate that smaller rBC particles (d_{ve} < 100 nm) from fresh fossil fuel combustion (vehicles) are not fully accounted for by bimodal lognormal fitting.[52] Similarly, fresh rBC particles derived from residential wood combustion may also be underestimated, leading to an overestimate of both MAC_{amb} and MAC_{TD}. Regardless of the exact reason for the small quantitative differences between the methods, the overall general behavior of E_{abs} and interpretation of the observations is method independent.

3.3 Optical properties of brown carbon aerosols

Knowledge of the imaginary part (k) of the complex refractive index for OA is needed to allow simulation of the climate impacts of absorbing OA particles.[7] Here, time-dependent k values for the total OA (k_{OA}) are determined at 405 nm by performing an optical closure analysis between observed and calculated values of E_{abs} (as opposed to absolute b_{abs} values).[21] The calculations are constrained by the observations of rBC-only (from the SP2) and PM_1 (from the SMPS) size distributions (Fig. S10) and the wavelength-dependent aerosol optical properties. The base case considered uses Mie theory assuming spherical particles with core-shell morphologies.

Information regarding the rBC coating state is required to fully separate contributions from internal mixing and BrC absorption and to elucidate the relationship between the mixing effect and coating amount. Since no direct coating state measurement is available from this study, time-dependent rBC effective coating thicknesses (or effective coating-to-core radius ratios, r_{coat}/r_{core}) are estimated from the $E_{abs,532nm}$ measurements via optical closure under the assumption that non-BC species do not absorb significantly at 532 nm and, thus, that $E_{abs,532nm}$ arises only from the mixing effect.[21] If BrC influences $E_{abs,532nm}$, then this method will overestimate the effective coating thickness and consequently the magnitude of the mixing effect at 405 nm, which will in turn lead to an underestimate of the BrC absorptivity. (The derived effective coating thicknesses may substantially underestimate the actual mean coating amount.[18])

Additional base case assumptions are as follows. The r_{coat}/r_{core} is assumed core-size independent, with effective diameters for the coated rBC particles determined by multiplying the rBC core diameters by r_{coat}/r_{core}. The size distributions for externally mixed PM_1 are

335 determined by subtracting the resulting coated rBC size distributions from the observed total
336 PM_1 size distributions. The complex RI for rBC is assumed to be $1.88 + 0.8i$.[18] All NR-PM_1
337 components, including OA, are assumed to be internally well mixed with a real RI of 1.50,
338 and all non-OA species are non-absorbing. The k values for the NR-PM_1 material in both BC-
339 containing and BC-free particles are determined from volume mixing rules. Thus, $k_{NR\text{-}PM1} =$
340 $f_{OA} \cdot k_{OA}$, where f_{OA} is the OA volume fraction. The f_{OA} values are determined from the
341 observed species-specific NR-PM_1 mass concentrations using the densities shown in Table S2.
342 The time-dependent k_{OA} values are retrieved by forcing optical closure (to within 1%)
343 between the observed and calculated $E_{abs,405nm}$ values. The overall retrieval process is
344 illustrated in Fig. S11.

345 In addition to the above base case, a variety of alternate cases are considered to assess the
346 sensitivity of the derived k_{OA} values to the model assumptions and measurement uncertainties,
347 with details provided in the *Supporting Information*. In brief, the sensitivity to morphology is
348 examined by assuming the BC core is an aggregate of individual (non-interacting) spherules
349 (either 40 or 70 nm) with Rayleigh-Debye-Gans (RDG) theory.[44] The sensitivity to the
350 assumed RI is examined by considering alternate values for BC or for the NR-PM_1
351 components. The sensitivity to the distribution of the coating material with respect to the BC
352 core size is tested by allowing for size-dependent variation in r_{coat}/r_{core}. The sensitivity to
353 measurement uncertainties in m_{rBC}, f_{OA} and $E_{abs,532nm}$ is examined by perturbing these up or
354 down by constant percentages. Each case is treated independently, and thus cross-sensitivities
355 are not assessed.

356 The base-case campaign average k_{OA} at 405 nm (from Mie) was 0.0046 ± 0.0055 (1σ),
357 with a pronounced diurnal profile and an average nighttime value of 0.008 (Fig. 4a). The

BBOA fraction of OA averaged ~22% at night, corresponding to a campaign-average k_{BBOA} of 0.037 at 405 nm under the assumption that BBOA is the only absorbing non-BC species. The retrieved nighttime k_{OA} values exhibit the largest sensitivity to uncertainties in m_{rBC}, f_{OA} and $E_{abs,532nm}$, with comparably small sensitivity to assumptions associated with particle morphology, RI or the coating distribution (Table 2 and Fig. S12-13). For example, a ±50% change in m_{rBC} corresponds to a ~±37% change in the nighttime k_{OA}, while the alternate morphology or coating distribution cases lead to changes of only a few percent.

Values for the OA-specific *MAC*, referred to as MAC_{OA}, are calculated as the ratio between the calculated OA-specific absorption (sum of internally and externally mixed OA) and the observed OA concentration. The nighttime MAC_{OA} (20:00-6:00) exhibits a reasonably linear relationship with the BBOA:OA ratio (Fig. 4b). Extrapolation of a Deming fit of MAC_{OA} versus BBOA:OA to BBOA:OA = 1 can provide an estimate of the BBOA-specific *MAC* (MAC_{BBOA}) at 405 nm. The extrapolated base-case MAC_{BBOA} = 0.60±0.02 $m^2\ g^{-1}$ if the fit is constrained to go through zero and is 0.53±0.01 $m^2\ g^{-1}$ if it is unconstrained with an intercept at BBOA:OA = 0 of 0.10 $m^2\ g^{-1}$. The estimated mean MAC_{BBOA} is an order of magnitude smaller than MAC_{BC}. The derived MAC_{BBOA} values exhibit similar sensitivities to the model assumptions as do the k_{OA} values, with, for example, a ±50% change in m_{rBC} yielding a ~±34% change in the MAC_{BBOA}. The MAC_{BBOA} can alternatively be estimated from the ratio between calculated OA absorption and [BBOA]; the mean from this method is similar to the constrained fit (Fig. 4c). The non-zero intercept from the unconstrained fit suggests the non-BBOA organic components (HOA, COA and OOA) are also slightly absorbing, although we suggest that it is more likely that this is simply a limitation of the data set and fitting, and that the *MAC* for these other OA components is close to zero.

The k_{BBOA} and MAC_{BBOA} determined here are compared with literature results from various laboratory and ambient studies in Table 1. The reported absorption characteristics of biomass burning aerosols vary greatly, likely due to differences between measurement techniques, burning conditions or extent of atmospheric processing. The k_{BBOA} and MAC_{BBOA} determined from this study are likely lower-limit values, since some fraction of BBOA may be non-absorbing (Fig. 3). However, this just illustrates the difficulty in clearly defining "brown" carbon, for example whether it should be considered as the total OA or just some fraction of the total OA (or even some sub-fraction of a given OA type).

The contributions from rBC absorption, absorption due to internal mixing (lensing), and direct absorption by BrC to the total observed $b_{abs,405nm}$ were on average 67.3%, 13.9% and 18.8% and at night were 56.3%, 14.2% and 29.5%, respectively (Fig. S14). These values depend on the relative contribution from biomass burning versus fossil fuel combustion, which vary with time of day and between days. Clearly, the fractional contribution of BrC to light absorption in even a single region is highly variable, which underscores the importance of accurate in-situ characterizations of BrC optical properties in multiple locations. Future studies would additionally benefit from direct measurement of the BC coating state and from comparison between optical measurements made using multiple methodologies. Although the BrC contribution was substantial at nighttime, it was overall negligible during the day, suggesting that BrC may not drive surface radiative forcing in Fresno in winter, although the export of this BrC throughout the wider SJV may be of regional importance. However, primary BrC aerosols from biomass burning sources often contain PAHs, nitrogen-containing aromatic compounds[53-54] and humic-like substances (HULIS),[55-56] which can exert negative effects on human health.[57-58]

Acknowledgement

We thank the CARB Fresno-Garland monitoring site for providing space and logistical help during the course of the study, and NASA for travel support and coordination of the larger DISCOVER-AQ study. Additional support was provided by the California Air Resources Board, Research Division, under Contract No. 13-330. CDC and XZ thank Gavin McMeeking at DMT for the PAX instrument and Haf Jonsson for facilitating the deployment of the SP2. QZ, HK and CP thank NASA and the California Agricultural Experiment Station (Project CA-D-ETX-2102-H) for supporting the acquisition and analysis of the AMS data. This work has not been formally reviewed by the funding agencies and represents the views of the authors.

Supporting Information

The Supporting Information includes additional tables and figures, as noted in the text. This information is available free of charge via the Internet at http://pubs.acs.org/.

References

1. Bond, T. C. et al. Bounding the role of black carbon in the climate system: A scientific assessment. *J Geophys. Res.* **2013**, *118*(11), 5380-5552; DOI 10.1002/jgrd.50171.

2. Ramanathan V.; Carmichael, G. Global and regional climate changes due to black carbon. *Nat. Geosci*. **2008**, 1, 221–227; DOI 10.1038/ngeo156.

3. Jacobson, M. Z. Global direct radiative forcing due to multicomponent anthropogenic and natural aerosols. *J. Geophys. Res*. **2001**, *106*, 1551–1568; DOI 10.1029/2000JD900514.

4. Fuller, K. A.; Malm, W. C.; Kreidenweis, S. M. Effects of mixing on extinction by carbonaceous particles. *J. Geophys. Res*. **1999**, *104*, 15941–15954; DOI 10.1029/1998JD100069.

5. Bond, T. C.; Habib, G.; Bergstrom, R. W. Limitations in the enhancement of visible light absorption due to mixing state. *J. Geophys. Res*. **2006**, *111*(D20), D20211; DOI 10.1029/2006JD007315.

6. Jacobson, M. Z. A physically based treatment of elemental carbon optics: Implications for global direct forcing of aerosols. *Geophys. Res. Lett.* **2000**, *27*, 217–220; DOI 10.1029/1999GL010968.

7. Andreae, M.; Gelencser, A. Black carbon or brown carbon? The nature of light absorbing carbonaceous aerosols. *Atmos. Chem. Phys*. **2006**, *6*, 3131-3148; DOI 10.5194/acp-6-3131-2006.

8. Barnard, J. C.; Volkamer, R.; Kassianov, E. I. Estimation of the mass absorption cross section of the organic carbon component of aerosols in the Mexico City Metropolitan Area. *Atmos. Chem. Phys.* **2009**, *8*, 6665–6679; DOI 10.5194/acp-8-6665-2008.

9. Kirchstetter, T. W.; Novakov, T.; Hobbs, P. V. Evidence that the spectral dependence of light absorption by aerosols is affected by organic carbon. *J. Geophys. Res*. **2004**, *109*(D21), D21208; DOI 10.1029/2004JD004999.

10. Updyke, K. M.; Nguyen, T. B.; Nizkorodov, S. A. Formation of brown carbon via reactions of ammonia with secondary organic aerosols from biogenic and anthropogenic precursors. *Atmos. Environ*. **2012**, *63*, 22-31; DOI 10.1016/j.atmosenv.2012.09.012.

11. Yang, M.; Howell, S. G.; Zhuang, J.; Huebert, B. J. Attribution of aerosol light absorption to black carbon, brown carbon, and dust in China - Interpretations of atmospheric measurements during EAST-AIRE. *Atmos. Chem. Phys*. **2009**, *9*, 2035-2050; DOI 10.5194/acp-9-2035-2009.

12. Zhang, X.; Lin, Y.-H.; Surratt, J. D.; Zotter, P.; Prévôt, A. H. S.; Weber, R. J. Light-absorbing soluble organic aerosol in Los Angeles and Atlanta: A contrast in secondary organic aerosol. *Geophys. Res. Lett.* **2011**, *38*, L21810; DOI 10.1029/2011GL049385.

13. Cross, E. S. et al. Soot particle studies-Instrument inter-comparison-Project overview. *Aerosol Sci. Technol*. **2010**, *44*, 592-611; DOI 10.1080/02786826.2010.482113.

14. Metcalf, A. R.; Loza, C. L.; Coggon, M. M.; Craven, J. S.; Jonsson, H. H.; Flagan, R. C.; Seinfeld, J. H. Secondary Organic Aerosol Coating Formation and Evaporation: Chamber

458 Studies Using Black Carbon Seed Aerosol and the Single-Particle Soot Photometer. *Aerosol*
459 *Sci. Technol*. **2013**, *47*(3), 326–347; DOI 10.1080/02786826.2012.750712.

460 15. Zhang, R.; Khalizov, A. F.; Pagels, J.; Zhang, D.; Xue, H.; McMurry, P. H. Variability in
461 morphology, hygroscopicity, and optical properties of soot aerosols during atmospheric
462 processing. *Proc. Natl. Acad. Sci.* **2008**, *105*, 10291-10296; DOI 10.1073/pnas.0804860105.

463 16. Lack, D. A.; Cappa, C. D. Impact of brown and clear carbon on light absorption
464 enhancement, single scatter albedo and absorption wavelength dependence of black carbon.
465 *Atmos. Chem. Phys.* **2010**, *10*(9), 4207-4220; DOI 10.5194/acp-10-4207-2010.

466 17. Wang, X.; Heald, C. L.; Ridley, D. A.; Schwarz, J. P.; Spackman, J. R.; Perring, A. E.;
467 Coe, H.; Liu, D.; Clarke, A. D. Exploiting simultaneous observational constraints on mass and
468 absorption to estimate the global direct radiative forcing of black carbon and brown carbon.
469 *Atmos. Chem. Phys*. **2014**, *14*, 10989-11010; DOI 10.5194/acp-14-10989-2014.

470 18. Cappa, C. D. et al. Radiative absorption enhancements due to the mixing state of
471 atmospheric black carbon. *Science* **2012**, *337*, 1078–1081; DOI 10.1126/science.1223447.

472 19. Liu, S.; Aiken, A. C.; Gorkowski, K.; Dubey, M. K.; Cappa, C. D.; WIlliams, L. R.;
473 Herndon, S. C.; Massoli, P.; Fortner, E. C.; Chhabra, P. S.; Brooks, W. A.; Onasch, T. B.;
474 Worsnop, D. R.; China, S.; Sharma, N.; Mazzoleni, C.; Xu, L.; Ng. N. L.; Liu, D.; Allan,J. D.;
475 Lee, J. D.; Fleming, Z. L.; Mohr, C.; Zotter, P.; Szidat, S.; Prevot, A. S. H. Enhanced light
476 absorption by mixed source black and brown carbon particles in UK winter. *Nat. Commun.*
477 **2015**, *6*:8435; DOI:10.1038/ncomms9435.

478 20. Healy, R. M.; Wang, J. M.; Jeong, C.-H.; Lee, A. K. Y.; Willis, M. D.; Jaroudi, E.;
479 Zimmerman, N.; Hilker, N.; Murphy, M.; Eckhardt, S.; Stohl, A.; Abbatt, J. P. D.; Wenger, J.
480 C.; Evans, G. J. Light-absorbing properties of ambient black carbon and brown carbon from
481 fossil fuel and biomass burning sources. *J. Geophys. Res*. **2015**, *120*, 6619-6633; DOI
482 10.1002/2015JD023382.

483 21. Lack, D. A.; Langridge, J. M.; Bahreini, R.; Cappa, C. D.; Middlebrook, A. M.; Schwarz,
484 J. P. Brown carbon and internal mixing in biomass burning particles. *Proc. Natl. Acad. Sci.*
485 **2012**, *109*, 14802-14807; DOI 10.1073/pnas.1206575109.

486 22. Bergstrom, R. W.; Pilewskie, P.; Russell, P. B.; Redemann, J.; Bond, T. C.; Quinn, P. K.;
487 Sierau, B. Spectral absorption properties of atmospheric aerosols *Atmos. Chem. Phys.* **2007**,
488 *7*(23), 5937-5943; DOI 10.5194/acp-7-5937-2007.

489 23. Kirchstetter, T. W.; Thatcher, T. L. Contribution of organic carbon to wood smoke
490 particulate matter absorption of solar radiation. *Atmos. Chem. Phys.* **2012**, *12*(14), 6067-6072;
491 DOI 10.5194/acp-12-6067-2012.

492 24. Bahadur, R.; Praveen, P. S.; Xu, Y.; Ramanathan, V. Solar absorption by elemental and
493 brown carbon determined from spectral observations. *Proc. Natl. Acad. Sci.* **2012**, *109*(43),
494 17366-17371; DOI 10.1073/pnas.1205910109.

495 25. Chung, C. E.; Ramanathan, V.; Decremer, D. Observationally constrained estimates of
496 carbonaceous aerosol radiative forcing. *Proc. Natl. Acad. Sci.* **2012**, *109*(29), 11624-11629;
497 DOI 10.1073/pnas.1203707109.

26. Gyawali, M.; Arnott, W. P.; Lewis, K.; Moosmüller, H. In situ aerosol optics in Reno, NV, USA during and after the summer 2008 California wildfires and the influence of absorbing and non-absorbing organic coatings on spectral light absorption. *Atmos. Chem. Phys.* **2009**, *9*(20), 8007-8015; DOI 10.5194/acp-9-8007-2009.

27. Knox, A.; Evans, G. J.; Brook, J. R.; Yao, X.; Jeong, C. H.; Godri, K. J.; Sabaliauskas, K.; Slowik, J. G. Mass Absorption Cross-Section of Ambient Black Carbon Aerosol in Relation to Chemical Age. *Aerosol Sci. Technol.* **2009**, *43*(6), 522-532; DOI 10.1080/02786820902777207.

28. Saleh, R.; Hennigan, C. J.; McMeeking, G. R.; Chuang, W. K.; Robinson, E. S.; Coe, H.; Donahue, N. M.; Robinson, A. L. Absorptivity of brown carbon in fresh and photo-chemically aged biomass-burning emissions. *Atmos. Chem. Phys.* **2013**, *13*, 7683–7693; DOI 10.5194/acp-13-7683-2013.

29. McMeeking, G.; Fortner, E.; Onasch, T. B.; Taylor, J.; Flynn, M.; Coe, H.; Kreidenweis, S. M. Impacts of non-refractory material on light absorption by aerosols emitted from biomass burning. *J. Geophys. Res.* **2014**, *119*, D021750; DOI 10.1002/2014JD021750.

30. Nakayama, T.; Ikeda, Y.; Sawada, Y.; Setoguchi, Y.; Ogawa, S.; Kawana, K.; Mochida, M.; Ikemori, F.; Matsumoto, K.; Matsumi, Y. Properties of light-absorbing aerosols in the Nagoya urban area, Japan, in August 2011 and January 2012: Contributions of brown carbon and lensing effect. *J. Geophys. Res.* **2014**, *119*, 12721-12739; DOI 10.1002/2014JD021744.

31. Cox, P.; Delao, A.; Komorniczak, A. The California almanac of emissions and air quality, *California Air Resource Board* **2013**, Sacramento, CA.

32. Ngo, M. et al. Airborne particles in the San Joaquin Valley may affect human health, *Calif. Agric*. **2010**, *64*(1), 12–16; DOI 10.3733/ca.v064n01p12.

33. Chow, J. C.; Chen, L. W. A.; Watson, J. G.; Lowenthal, D. H.; Magliano, K. A.; Turkiewicz, K.; Lehrman, D. E. PM2.5 chemical composition and spatiotemporal variability during the California Regional PM10/PM2.5 Air Quality Study (CRPAQS). *J. Geophys. Res.* **2006**, *111*, D10S04; DOI 10.1029/2005JD006457.

34. Chow, J. C.; Watson, J. G.; Lowenthal, D. H.; Chen, L. W. A.; Zielinska, B.; Mazzoleni, L. R.; Magliano, K. L. Evaluation of organic markers for chemical mass balance source apportionment at the Fresno Supersite. *Atmos. Chem. Phys*. **2007**, *7*(7), 1741–1754; DOI 10.5194/acp-7-1741-2007.

35. Chen, L. W. A.; Watson, J. G.; Chow, J. C.; Magliano, K. L. Quantifying PM2.5 source contributions for the San Joaquin Valley with multivariate receptor models. *Environ. Sci. Technol*. **2007**, *41*(8), 2818–2826; DOI 10.1021/es0525105.

36. Magliano, K. L.; Hughes, V. M.; Chinkin, L. R.; Coe, D. L.; Haste, T. L.; Kumar, N.; Lurmann, F. W. Spatial and temporal variations in PM10 and PM2.5 source contributions and comparison to emissions during the 1995 integrated monitoring study. *Atmos. Environ.* **1999**, *33*(29), 4757–4773; DOI 10.1016/S1352-2310(99)00265-4.

37. Ge, X.; Setyan, A.; Sun, Y.; Zhang, Q. Primary and secondary organic aerosols in Fresno, California during wintertime: Results from high resolution aerosol mass spectrometry. *J. Geophys. Res.* **2012**, *117*(D19), D19301; DOI 10.1029/2012JD018026.

38. Young, D. E.; Kim, H.; Parworth, C.; Zhou, S.; Zhang, X.; Cappa, C. D.; Seco, R.; Kim, S.; Zhang, Q. Influences of emission sources and meteorology on aerosol chemistry in a polluted urban environment: results from DISCOVER-AQ California. *Atmos. Chem. Phys. Discuss.* **2015**, *15*, 35057-35115; DOI 10.5194/acpd-15-35057-2015.

39. Cappa, C. D.; Che, D. L.; Kessler, S. H.; Kroll, J. H.; Wilson, K. R. Variations in organic aerosol optical and hygroscopic properties upon heterogeneous OH oxidation. *J. Geophys. Res*. **2011**, *116*, D15204; DOI 10.1029/2011jd015918.

40. Langridge, J. M.; Richardson, M. S.; Lack, D.; Law, D.; Murphy, D. M. Aircraft instrument for comprehensive characterization of aerosol optical properties, Part I: Wavelength-dependent optical extinction and its relative humidity dependence measured using cavity ringdown spectroscopy. *Aerosol Sci. Technol*. **2011**, *45*, 1305-1318; DOI 10.1080/02786826.2011.592745.

41. Lack, D. A.; Richardson, M. S.; Law, D.; Langridge, J. M.; Cappa, C. D.; McLaughlin, R. J.; Murphy, D. M. Aircraft instrument for comprehensive characterization of aerosol optical properties, Part 2: Black and brown Carbon absorption and absorption Enhancement measured with photo acoustic spectroscopy. *Aerosol Sci. Technol*. **2012**, *46*, 555-568; DOI 10.1080/02786826.2011.645955.

42. Schwarz, J. P.; Gao, R. S.; Fahey, D. W.; Thomson, D. S.; Watts, L. A.; Wilson, J. C.; Reeves, J. M.; Darbeheshti, M.; Baumgardner, D. G.; Kok, G. L.; Chung, S. H.; Schulz, M.; Hendricks, J.; Lauer, A.; Karcher, B.; Slowik, J. G.; Rosenlof, K. H.; Thompson, T. L.; Langford, A. O.; Loewenstein, M.; Aikin, K. C. Single-particle measurements of midlatitude black carbon and light-scattering aerosols from the boundary layer to the lower stratosphere. *J. Geophys. Res.* **2006**, *111*, D16207; DOI 10.1029/2006JD007076.

43. Laborde, M.; Mertes, P.; Zieger, P.; Dommen, J.; Baltensperger, U.; Gysel, M. Sensitivity of the Single Particle Soot Photometer to different black carbon types. *Atmos. Meas. Technol*. **2012**, *5*, 1031-1043; DOI 10.5194/amt-5-1031-2012.

44. Bond, T. C.; Bergstrom R. W. Light absorption by carbonaceous particles: an investigative review. *Aerosol Sci. Technol*. **2006**, *40*, 27–67; DOI 10.1080/02786820500421521.

45. Canagaratna, M.; Jayne, J.; Jimenez, J. L.; Allan, J. A.; Alfarra, R.; Zhang, Q.; Onasch, T.; Drewnick, F.; Coe, H.; Middlebrook, A.; Delia, A.; Williams, L.; Trimborn, A.; Northway, M.; DeCarlo, P.; Kolb, C.; Davidovits, P.; Worsnop, D. Chemical and microphysical characterization of ambient aerosols with the aerodyne aerosol mass spectrometer. *Mass Spectrom. Rev*. **2007**, *26*, 185-222; DOI 10.1002/mas.20115.

46. Zhang, Q.; Jimenez, J. L.; Canagaratna, M.; Ng, N. L.; Ulbrich, I.; Worsnop, D.; Sun, Y. L. Understanding organic aerosols via factor analysis of aerosol mass spectrometry: A review. *Anal. Bioanal. Chem.* **2011**, *401*, 3045-3067; DOI 10.1007/s00216-011-5355-y.

47. Schneider, J.; Weimer, S.; Drewnick, F.; Borrmann, S.; Helas, G.; Gwaze, P.; Schmid, O.; Andreae, M. O.; Kirchner, U. Mass spectrometric analysis and aerodynamic properties of various types of combustion-related aerosol particles. *Int. J. Mass. Spec*. **2006**, *258*, 37–49; DOI 10.1016/ j.ijms.2006.07.008.

48. Alfarra, M. R.; Prévôt, A. H. S.; Szidat, S.; Sandradewi, J.; Weimer, S.; Lanz, V. A.;

581 Schreiber, D.; Mohr, M.; Baltensperger, U. Identification of the mass spectral signature of
582 organic aerosols from wood burning emissions. *Environ. Sci. Technol*. **2007**, *41*(16), 5770–
583 5777; DOI 10.1021/es062289b.

584 49. Chen, Y.; Bond, T. C. Light absorption by organic carbon from wood combustion. *Atmos.*
585 *Chem. Phys*. **2010**, *10*, 1773–1787; DOI 10.5194/acp-10-1773-2010.

586 50. Bruns, E. A.; Krapf, M.; Orasche, J.; Huang, Y.; Zimmermann, R.; Drinovec, L.; Mocnik,
587 G.; El-Haddad, I.; Slowik, J. G.; Dommen, J.; Baltensperger, U.; Prévôt, A. H. S.
588 Characterization of primary and secondary wood combustion products generated under
589 different burner loads. *Atmos. Chem. Phys.* **2015**, *15*, 2825-2841; DOI 10.5194/acp-15-2825-
590 2015.

591 51. U.S.EPA. Report to congress on black carbon. **2012**, Agency, U.S.E.P.A., Washington
592 DC. http://www.epa.gov/blackcarbon/.

593 52. Buffaloe, G. M.; Lack, D. A.; Williams, E. J.; Coffman, D.; Hayden, K. L.; Lerner, B. M.;
594 Li, S-M.; Nuaaman I.; Massoli, P.; Onasch, T. B.; Quinn, P. K.; Cappa, C. D. Black carbon
595 emissions from in-use ships: a California regional assessment. *Atmos. Chem. Phys*. **2014**, *14*,
596 1881-1896; DOI 10.5194/acp-14-1881-2014.

597 53. Mohr, C.; Lopez-Hilfiker, F. D.; Zotter, P.; Prévôt, A. S. H.; Xu, L.; Ng, N. L.; Herndon,
598 S. C.; Williams, L. R.; Franklin, J. P.; Zahniser, M. S.; Worsnop, D. R.; Knighton, W. B.;
599 Aiken, A. C.; Gorkowski, K. J.; Dubey, M. K.; Allan, J. D.; Thornton, J. A. Contribution of
600 Nitrated Phenols to Wood Burning Brown Carbon Light Absorption in Detling, United
601 Kingdom during Winter Time. *Environ. Sci. Technol*. **2013**, *47* (12), 6316–6324;
602 DOI 10.1021/es400683v.

603 54. Desyaterik, Y.; Sun, Y.; Shen, X.; Lee, T.; Wang, X.; Wang T.; Collett Jr., J. L.
604 Speciation of "Brown" Carbon in Cloud Water Impacted by Agricultural Biomass Burning in
605 Eastern China. *J. Geophys. Res.* **2013**, *118*, 7389-7399; DOI 10.1002/jgrd.50561.

606 55. Hoffer, A.; Gelencser, A.; Guyon, P.; Kiss, G.; Schmid, O.; Frank, G. P.; Artaxo, P.;
607 Andreae, M. O. Optical properties of humic-like substances (HULIS) in biomass-burning
608 aerosols. *Atmos. Chem. Phys*. **2006**, *6*, 3563-3570; DOI 10.5194/acp-6-3563-2006.

609 56. Lukacs, H.; Gelencser, A.; Hammer, S.; Puzbaum, H.; Pio, C.; Legrand, M.; Kasper-
610 Giebl, A.; Handler, M.; Limbeck, A.; Simpson, D.; Preunkert, S. Seasonal trends and possible
611 sources of brown carbon based on 2-year aerosol measurements at six sites in Europe. *J.*
612 *Geophys. Res*. **2007**, *112*, D23S18; DOI 10.1029/2006JD008151.

613 57. Huang, Q. G.; Wang, L. S.; Han, S. K. The genotoxicity of substituted nitrobenzenes and
614 the quantitative structure-activity relationship studies. *Chemosphere* **1995**, *30*(5), 915−923;
615 DOI 10.1016/0045-6535(94)00450-9.

616 58. Verma, V.; Rico-Martinez, R.; Kotra, N.; King, L.; Liu, J.; Snell, T. W.; Weber, R. J.
617 Contribution of water-soluble and insoluble components and their hydrophobic/hydrophilic
618 subfractions to the reactive oxygen species-generating potential of fine ambient aerosols.
619 *Environ. Sci. Technol*. **2012**, *46*, 11384-11392; DOI 10.1021/es302484r.

620 59. Chakrabarty, R. K.; Moosmüller, H.; Chen, L.-W. A.; Lewis, K.; Arnott, W. P.;
621 Mazzoleni, C.; Dubey, M. K.; Wold, C. E.; Hao, W. M.; Kreidenweis, S. M. Brown carbon in

622 tar balls from smoldering biomass combustion. *Atmos. Chem. Phys*. **2010**, *10*, 6363–6370;
623 DOI 10.5194/acp-10-6363-2010.

624 60. Wandinger, U.; Müller, D.; Bockmann, C.; Althausen, D.; Matthias,V.; Bösenberg, J.;
625 Weiss, V.; Fiebig, M.; Wendisch, M.; Stohl, A.; Ansmann, A. Optical and micro10 physical
626 characterization of biomass-burning and industrial-pollution aerosols from multiwavelength
627 lidar and aircraft measurements. *J. Geophys. Res.* **2002**, *107*(D21), 8125; DOI
628 10.1029/2000JD000202.

629 61. Adler, G.; Flores, J. M.; Abo Riziq, A.; Borrmann, S.; Rudich, Y. Chemical, physical, and
630 optical evolution of biomass burning aerosols: a case study. *Atmos. Chem. Phys*. **2011**, *11*,
631 1491–1503; DOI 10.5194/acp-11-1491-2011.
632

633 **Table 1.** Published values of the imaginary part of the complex refractive index (k_{BBOA}) and
634 the mass absorption cross-section (MAC_{BBOA}) of the OA components of wood burning
635 aerosols, excluding BC contributions.

636

	λ , nm	k_{BBOA}	MAC_{BBOA} $m^2\ g^{-1}$	Optical Measurement	Aerosol type sampled	Sampling Location	Literature
Laboratory	550	0.02-0.06		Aethalometer	Oak burning POA	-	[28]
	550	0.015-0.04		Aethalometer	Pocosin Pine burning POA	-	[28]
	550	0.0055-0.022		Aethalometer	Galberry burning POA	-	[28]
	400	0.038	1.1	UV/Vis (filter methanol extracts)	Pine/Oak wood burning	-	[49]
	405	0.015		Photo-Acoustic Spectrometer	Tar balls from Ponderosa Pine Duff burning	-	[59]
	405	0.0076		Photo-Acoustic Spectrometer	Tar balls from Alaskan Duff burning	-	[59]
Ambient	404	0.01	1.0-1.1	Photo-Acoustic Spectrometer	Wild fire, near-source emission	Four Mile Canyon, Colorado	[21]
	470		1.01	Aethalometer	Biomass burning influenced	Beijing, China	[11]
	400	0.112	2.9	Light transmission (filter)	Wood burning and biomass smoke aerosols	Savanna	[9]
	532	0.0016-0.0019	0.029-0.031	Photo-Acoustic Spectrometer	HULIS from biomass burning aerosols	Amazon basin	[55]
	Broadband	0.05-0.07		Airborne lidar	Upwind of forest fires	Northern Canada	[60]
	Broadband	0.07±0.03/ 0.04±0.01		White light optical particle counter	Open fire/ Smoldering phase	Urban Rehovot, Israel	[61]
This study	405	0.037	0.53 or 0.60	Photo-Acoustic Spectrometer	Biomass burning influenced	Fresno, CA	-

637

638

Table 2. Uncertainty (% change) in the retrieved k_{OA} resulted from the model assumptions (spherical particle shape, refractive indices of black carbon (BC) and non-BC particles) and measurement uncertainties associated with refractory BC mass, organic aerosol volume fraction and absorption enhancement.

Assumption/Parameter	Base case	Alternate case	% change in k_{OA}*
Spherical Particle Shape	Mie	RDG (40 nm)	-2.2%
		RDG (70 nm)	+5.9%
Coating Distribution	Constant r_{coat}/r_{core}	Diffusion-controlled growth of the coating materials on rBC core	-2.8%
RI (n, k) for BC	1.88-0.8i	1.75-0.63i	-12.4%
RI (n) of non-BC particles	1.50	+0.05	-5.4%
		-0.05	+3.8%
rBC mass concentration (m_{rBC})	as measured	+30%	+19.1%
		-30%	-24.0%
		+50%	+35.8%
		-50%	-37.6%
Organic aerosol volume fraction (f_{OA})	as measured	+20%	-17.5%
		-20%	+13.6%
Absorption Enhancement at 405 and 532 nm (E_{abs})	as measured	+5%	-4.6%
		-5%	1.1%

* Percentage (%) change in the campaign-average k_{OA} value averaged between 23:00 and 2:00 relative to that derived from the base case

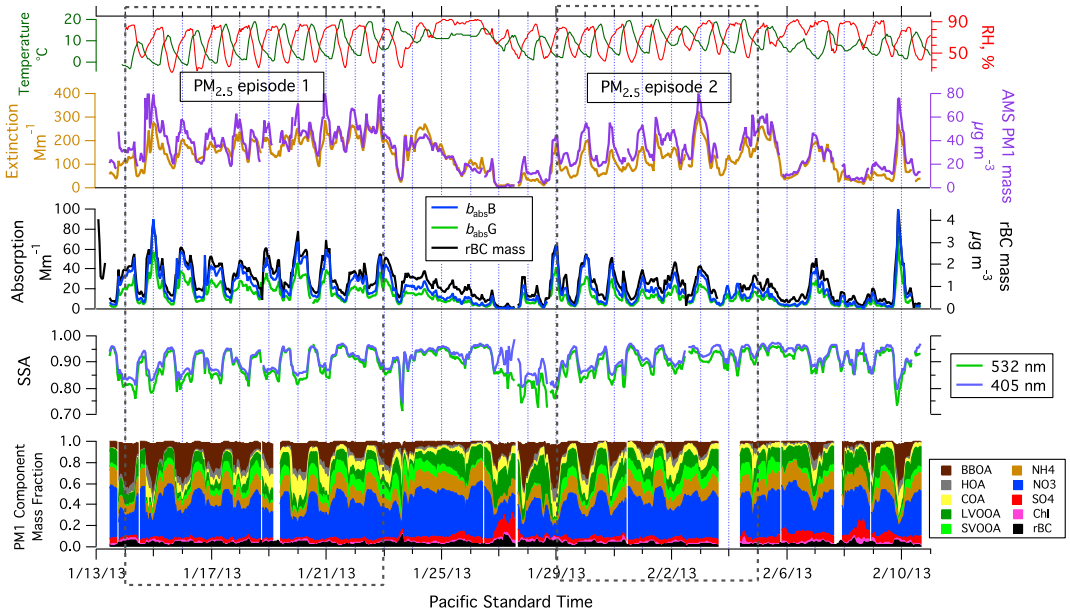

Figure 1. Time series of ambient temperature and relative humidity (RH), dry $PM_{2.5}$ light extinction coefficients at 532 nm, total PM_1 mass, dry $PM_{2.5}$ light absorption coefficients at 405 nm ($b_{abs}B$) and 532 nm ($b_{abs}G$), SP2 refractory black carbon (rBC) mass, single scattering albedo (SSA) at 405 and 532 nm, and the fractional composition of AMS PM_1 components during the DISCOVER-AQ 2013 California campaign in Fresno. Two $PM_{2.5}$ episodes with substantially elevated ground $PM_{2.5}$ concentrations, 1/14 – 1/23 and 1/29 – 2/5, are identified and labeled in the time series plot.

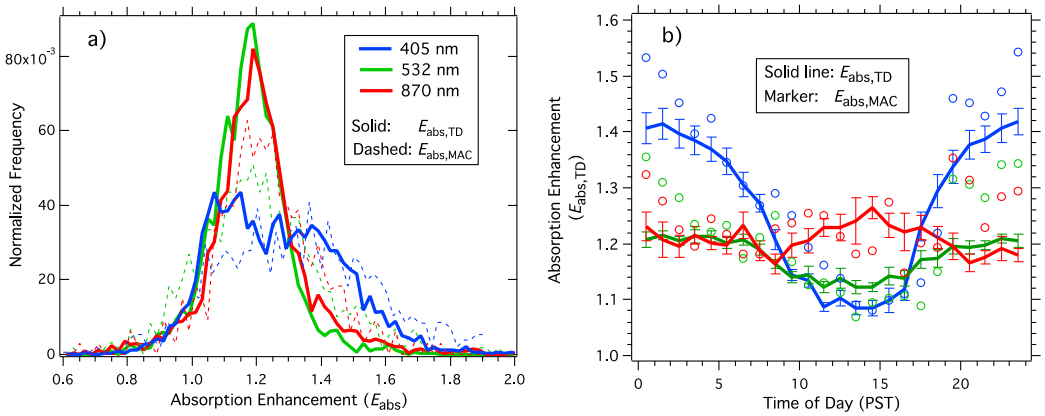

656

657 **Figure 2.** Normalized frequency distributions (a) and diurnal trends (b) of the measured $PM_{2.5}$
658 absorption enhancements using the TD method ($E_{abs,TD}$) and using the mass absorption cross-
659 section method ($E_{abs,MAC}$) at 405, 532 and 870 nm during DISCOVER-AQ. The $E_{abs,MAC}$
660 values were determined by normalizing the *MAC* of the ambient particles (MAC_{amb}) to the
661 average *MAC* of the thermo-denuded particles (MAC_{TD}) during the period between 13:00 and
662 16:00 (PST). Error bars shown for the $E_{abs,TD}$ in (b) are 1 standard error of the mean (SEM).

663

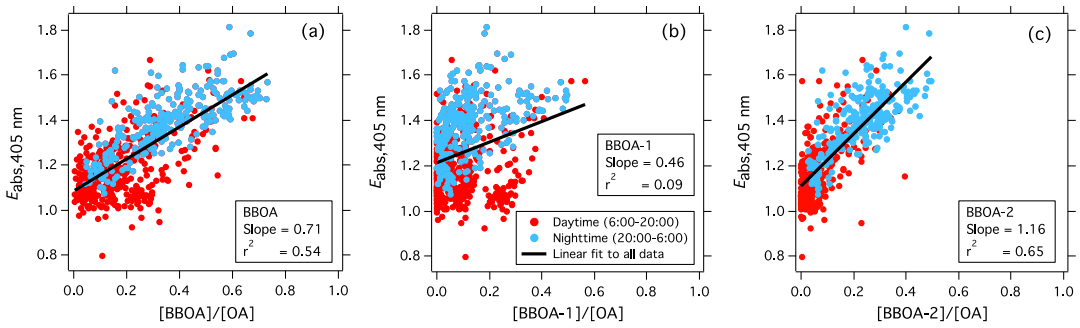

664

665 **Figure 3.** Scatter plots of the measured $PM_{2.5}$ absorption enhancement at 405 nm ($E_{abs,405nm}$)
666 versus the AMS BBOA:OA ratio (a), $E_{abs,405nm}$ versus BBOA-1:OA ratio (b), and $E_{abs,405nm}$
667 versus BBOA-2:OA ratio (c). Data were split into daytime (6:00-20:00, red) and nighttime
668 (20:00-6:00, blue). The slopes given in the scatter plots are determined from a one-sided
669 linear regression of the data in each panel (daytime + nighttime data).

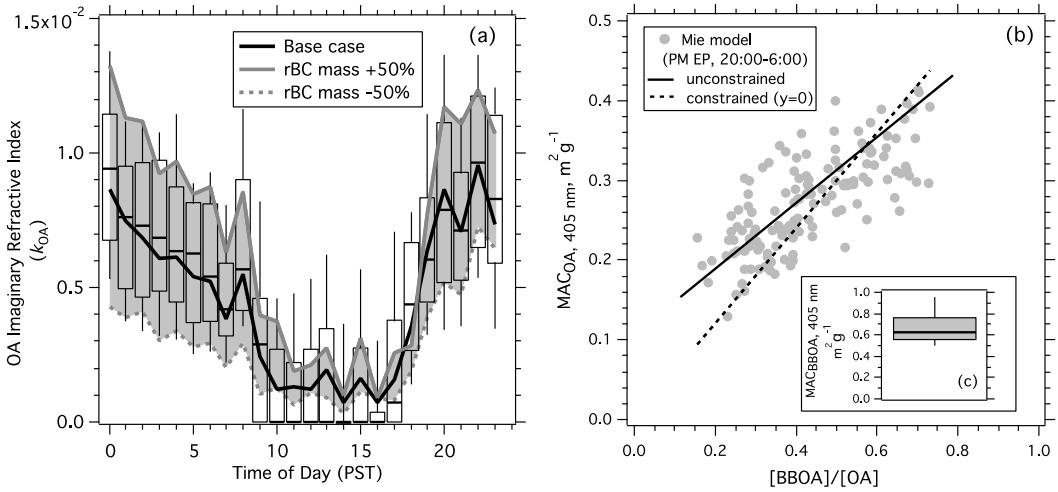

Figure 4. (a) Diurnal variation of the retrieved imaginary refractive index for organic aerosols (k_{OA}) (Mie model base case) (solid black line). The median value (thick horizontal bar), 25th and 75th percentiles (lower and upper box bounds, respectively), and 10th and 90th percentiles (lower and upper whiskers, respectively) of the k_{OA} are shown in the box and whisker plot. The uncertainty in the retrieved k_{OA} is assessed through sensitivity tests. Shown here as the upper and lower bounds of the shaded grey areas are the uncertainties in k_{OA} associated with ± 50% measurement uncertainty in the rBC mass. (b) Scatter plot of the mass absorption cross-section of the organic aerosol (MAC_{OA}) at 405 nm versus the AMS biomass burning organic aerosol (BBOA)-to-OA mass ratio. Only the nighttime (20:00-6:00) data during the two PM episodes are included. The lines show Deming regression fits to the data where the fit has been constrained to go through the origin (dashed) or unconstrained (solid). (c, inset) Box and whisker plot showing the variation in the MAC_{BBOA} values derived by taking the ratio of MAC_{OA} and [BBOA]:[OA].

Supporting Information

Optical Properties of Wintertime Aerosols from Residential Wood Burning in Fresno, CA: Results from DISCOVER-AQ 2013

Xiaolu Zhang[1], Hwajin Kim[2,3], Caroline Parworth[2], Dominique Young[2], Qi Zhang[2], Andrew R. Metcalf[4], Christopher D. Cappa[1,*]

[1]Department of Civil and Environmental Engineering, University of California, Davis, CA 95616

[2]Department of Environmental Toxicology, University of California, Davis, CA 95616

[3] Now at: Center for Environment, Health and Welfare Research, Korea Institute of Science and Technology, Seoul 136-701, Republic of Korea

[4]Department of Mechanical Engineering, University of Minnesota, Minneapolis, MN 55455

[*] Corresponding author

Email: cdcappa@ucdavis.edu

Phone: (530) 752-8180

Address: Department of Civil and Environmental Engineering, 3135 Ghausi Hall, University of California, One Shields Avenue, Davis, CA 95616

Number of Pages: 20
Number of Supplemental Figures: 14
Number of Supplemental Tables: 2

Sensitivity tests of the optical closure analysis:

In addition to the base case, a variety of alternate cases are considered to assess the sensitivity of the derived k_{OA} values to the model assumptions and measurement uncertainties. In one case, the model assumption on the spherical-particle shape has been evaluated by performing closure calculations using Rayleigh-Debye-Gans (RDG) theory, since Mie theory is known to underestimate the absorption of non-spherical BC particles.[1] With RDG, the BC core is assumed to be an aggregate of individual (non-interacting) spherules. The total absorption by each BC aggregate is the sum of the absorption by the individual spherules.[2] Here, spherule sizes ($D_{p,sph}$) of 40 and 70 nm have been considered. For the coated particles, we similarly assume that the total absorption is the sum over individual coated spherules and that the coating thickness is the same for each spherule.[3]

In another set of sensitivity tests, in calculating the effective coating thicknesses, instead of assuming a constant refractory black carbon (rBC) coating-to-core radius ratio (r_{coat}/r_{core}) across all particle sizes, the distribution of the non-refractory (NR) coating materials is assumed to follow a diffusion-controlled growth law:[4]

$$\frac{dD_p}{dt} = \frac{1}{D_p}$$

where D_p is the rBC volume equivalent diameter (d_{ve}). A previous laboratory study[5] on the evolution of rBC coating formation found good agreement between the modeled and measured coating thickness diameters when diffusion controlled growth was assumed. Like the base case (constant r_{coat}/r_{core}), the time-varying, size-dependent distributions of coating thicknesses across the rBC core distribution were obtained by constraining the

calculated $E_{abs,532nm}$ due to internal mixing to the observed $E_{abs,532nm}$, i.e. via optical closure.

The influence of the assumed rBC refractive index was tested by comparing rBC absorption coefficients ($b_{asb,BC}$) calculated using spherical-particle Mie theory for five alternate RI values with those calculated from the base case value (1.88-0.8*i*). The five RI values used are provided in Table 5 and are from *Bond and Bergstrom*.[1] Based on the slopes of the linear fits (Fig. S11), the $b_{asb,BC}$ determined from all five alternate RI values agree with the base case $b_{asb,BC}$ to within 11%. The largest difference from the base case is obtained for the RI = 1.75-0.63*i* case. Since this case gives the largest deviation in the calculated $b_{abs,BC}$, the difference between the retrieved k_{OA} value using this case (RI = 1.75-0.63*i*) versus the base case was assessed (Table 2, Figure S13).

The sensitivity of the retrieved k_{OA} to the assumed real component of the refractive index (n) of the non-BC components was assessed by using values of 1.45 and 1.55, compared to the base case value of 1.50.

Table 2 summarizes the uncertainties associated with measurements of rBC mass, m_{rBC}, volume fraction of organic aerosols, f_{OA}, and absorption enhancement, E_{abs}. In the sensitivity tests on the measurement uncertainties, the measured values of these input parameters were varied up and down by constant percentages (±30% and 50% for m_{rBC}, ±20% for f_{OA} and ±5% for E_{abs}).

Reference:

1. Bond, T. C.; Bergstrom R. W. Light absorption by carbonaceous particles: an investigative review. *Aerosol Sci. Technol.* **2006**, *40*, 27–67; DOI 10.1080/02786820500421521.

2. Sorensen, C. M. Light Scattering by Fractal Aggregates: A Review. *Aerosol Sci. Technol*. **2001**, *35*, 648–687; DOI 10.1080/02786820117868.

3. Liu, D.; Taylor, J. W.; Young, D. E.; Flynn, M. J.; Coe, H.; Allan, J. D. The effect of complex black carbon microphysics on the determination of the optical properties of brown carbon. *Geophys. Res. Lett.* **2015**, *42*, 613-619; DOI 10.1002/2014GL062443.

4. Seinfeld, J. H.; Pandis, S. N. Atmospheric chemistry and physics: From air pollution to climate change. **2006**, 2nd ed., John Wiley & Sons, Inc., New York.

5. Metcalf, A. R.; Loza, C. L.; Coggon, M. M.; Craven, J. S.; Jonsson, H. H.; Flagan, R. C.; Seinfeld, J. H. Secondary organic aerosol coating formation and evaporation: Chamber studies using black carbon seed aerosol and the single-particle soot photometer. *Aerosol Sci. Technol*. **2013**, *47*(3), 326–347; DOI 10.1080/02786826.2012.750712.

Table S1. Summary of the instrumentation, size cut and the measurements made at the Fresno ground site during DISCOVER-AQ.

Instrumentation	Size cut	Measurement
Cavity ringdown Spectrometer (**CRD**)	$PM_{2.5}$	Dry particle light extinction (b_{ext}) at 405 and 532 nm
Photoacoustic Spectrometer (**PAS**)	$PM_{2.5}$	Dry particle light absorption (b_{abs}) at 405 and 532 nm
Photoacoustic Extinctiometer (**PAX**)	$PM_{2.5}$	Dry particle light extinction (b_{ext}) and absorption (b_{abs}) at 870 nm
Single Particle Soot Photometer (**SP2**)	$PM_{2.5}$	Refractory black carbon (rBC) mass and number size distributions at size range of [100,300nm] (extrapolated to [20,1000nm] in the post analysis)
High Resolution Time-of-Flight Aerosol Mass Spectrometer (**HR-ToF-AMS**)	PM_1	Non refractory submicron particle (NR-PM_1) mass and chemical composition
Scanning Mobility Particle Sizer (**SMPS**)	PM_1	Particle number size distribution (16 - 685 nm)
Aerodynamic Particle Sizer (**APS**)	$PM_{2.5}$	Particle number size distribution (0.8 -2.5 μm)
Thermodenuder (**TD**)	$PM_{2.5}$	Absorption Enhancement (E_{abs}) at 405, 532 and 870 nm

Table S2. Density values of the PM_1 components used in the optical closure calculation.

Component	Density, g cm^{-3}
NH_4NO_3	1.72[a]
$(NH_4)_2SO_4$	1.77[a]
NaCl	2.16[a]
BC	1.80[b]
Organics	[c]

[a]from "Properties of the Elements and Inorganic Compounds", in CRC Handbook of Chemistry and Physics, Internet Version 2005, David R. Lide, ed., <http://www.hbcpnetbase.com>, CRC Press, Boca Raton, FL, 2005.

[b]adopted from Bond and Bergstrom[1]

[c]determined from the ratio of organic aerosol mass and the difference between the total aerosol volume determined with an SMPS and the sum of the volumes of the individual inorganic components.

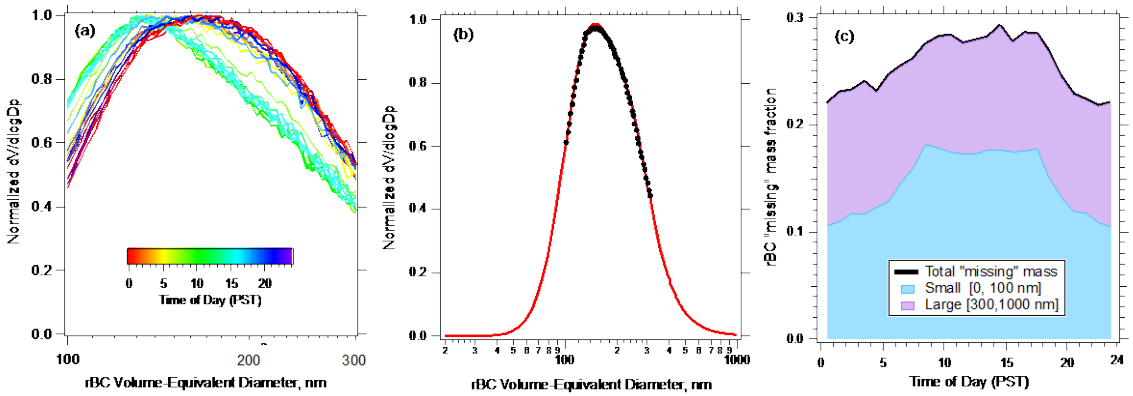

Figure S1. (a) Volume-weighted size distribution for refractory black carbon (rBC) determined from the SP2 measurements, averaged and colored by hour of day, (b) campaign-average rBC volume-weighted size distribution (black markers) during DISCOVER-AQ; the red dashed solid line represents the bimodal log-normal fit to the observation for the volume-equivalent diameter (d_{ve}) range of 20 to 1000 nm, and (c) the diurnal profile of the mass fraction of the rBC "missing" mass, calculated as the ratio between the rBC mass that is outside the SP2 detection window (100-300 nm) and the rBC mass determined from the lognormal fit (solid red line in Fig. S1b). The fractions of the total rBC mass that are attributable to "missing" mass from the smaller rBC particles (20 nm < d_{ve} < 100 nm) and from the bigger rBC particles (300 nm < d_{ve} < 1000 nm) are shown separately in the figure. The "missing" mass correction increases the total rBC mass by ~26% on average, with larger corrections during the daytime than at nighttime.

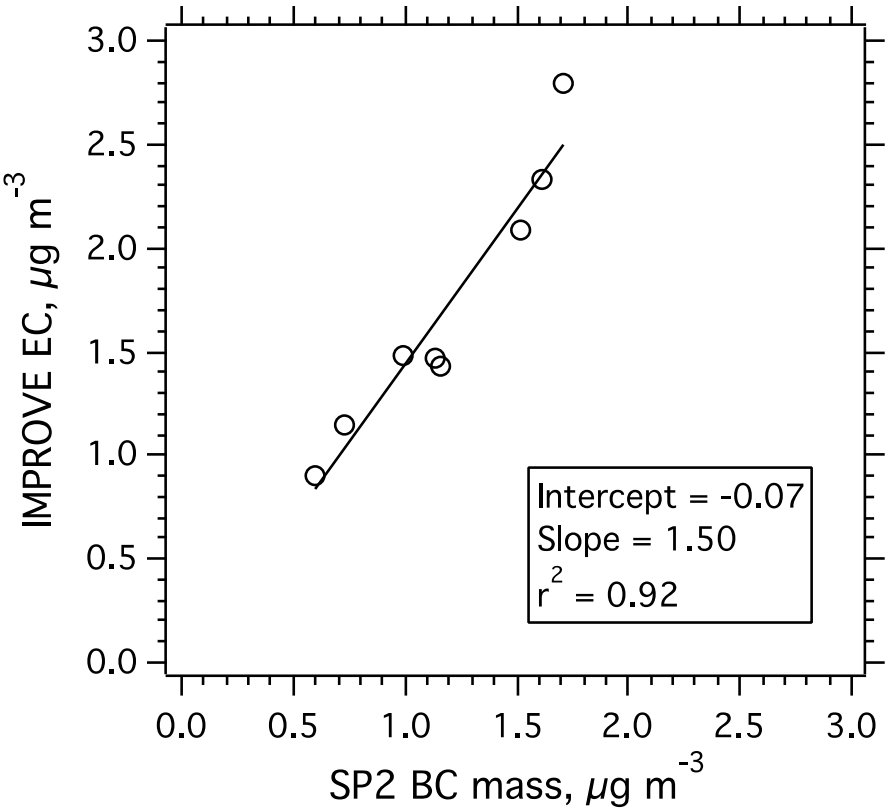

Figure S2. Scatter plot of the IMPROVE elemental carbon (EC) mass concentrations versus the daily-average SP2 refractory black carbon (BC) mass concentrations for the days that EC data were available during DISCOVER-AQ.

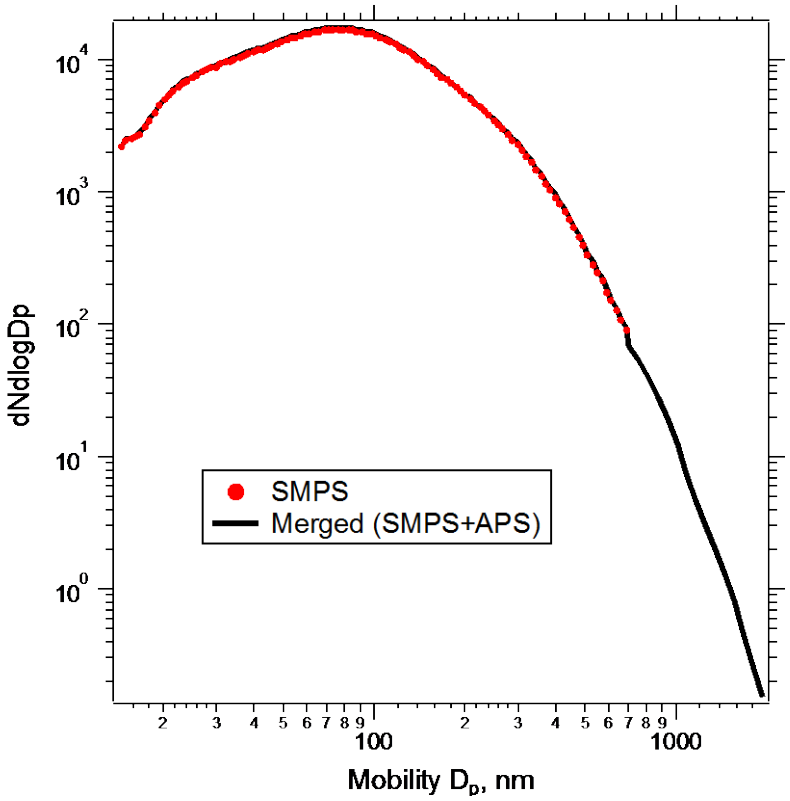

Figure S3. Campaign-average size distributions of ambient $PM_{2.5}$ from the scanning mobility particle sizer (SMPS) (red marker) and merged SMPS + aerodynamic particle sizer (APS) (black line) measurements.

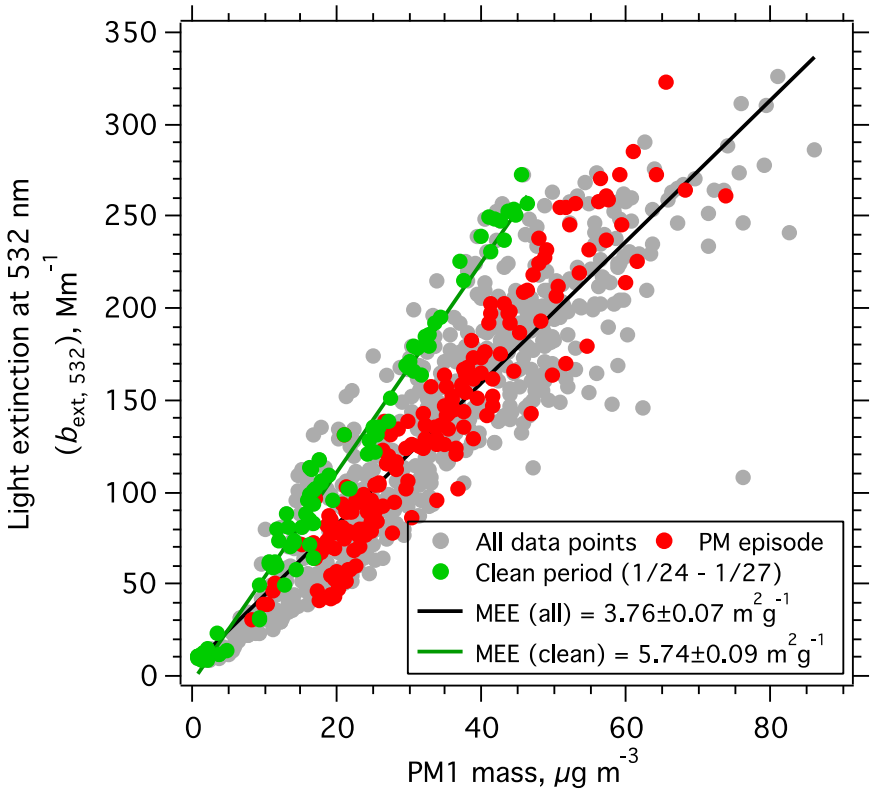

Figure S4. Scatter plot of $PM_{2.5}$ light extinction coefficients at 532 nm versus the PM_1 mass concentrations. The gray, red and green markers represent all data, data during the two PM episodes, and data during a clean period (1/24-1/27). The slopes of the Deming regression fits of the data yield the $PM_{2.5}$ mass extinction coefficient (MEC) (±1 standard deviation).

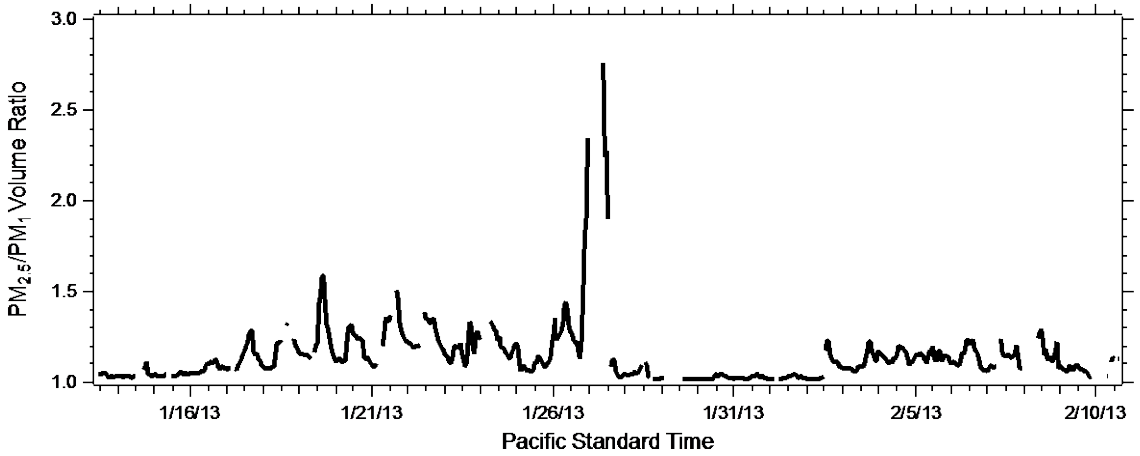

Figure S5. Time series of the $PM_{2.5}/PM_1$ volume ratio. Values >>1 correspond to periods with substantial contributions from supermicron particles to the total $PM_{2.5}$ volume concentration, with particularly large supermicron contributions observed on 27 January during the "clean" period. PM_1 volume is determined from the ambient SMPS size distribution measurements, while $PM_{2.5}$ volume is determined from the merged ambient SMPS+APS size distribution measurements. The gaps in the data are due to instrumentation issues.

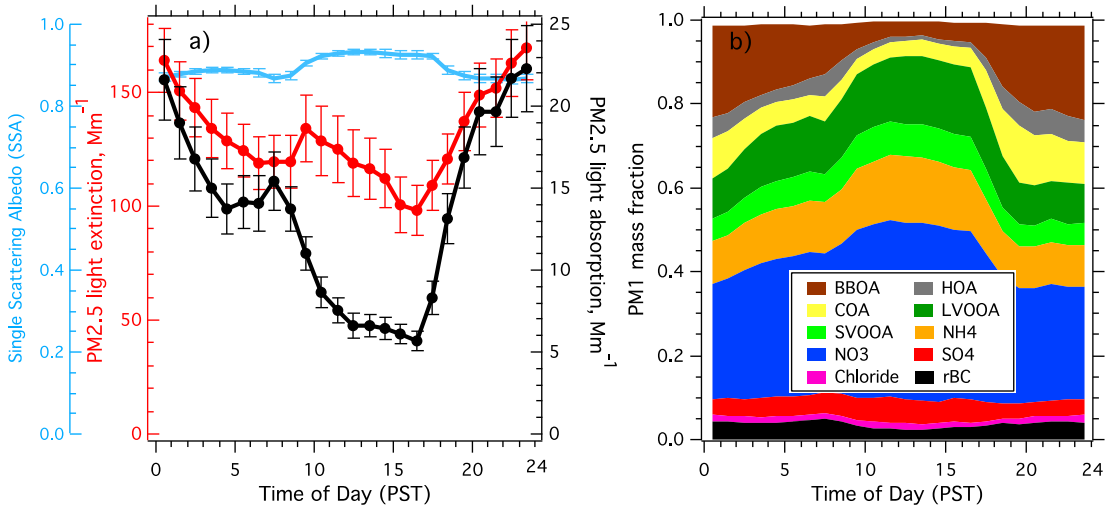

Figure S6. Campaign-average diurnal profiles of (a) $PM_{2.5}$ light extinction (b_{ext}), absorption coefficients (b_{abs}) and single scattering albedo (SSA) at 532nm determined from CRD-PAS measurements and (b) the fractional contribution of PM_1 inorganic and organic aerosols determined from AMS measurements. The organic factors, i.e. biomass burning organic aerosol (BBOA), hydrocarbon-like organic aerosol (HOA), cooking organic aerosol (COA), low-volatility oxygenated organic aerosol (LVOOA) and semi-volatile oxygenated organic aerosol (SVOOA), are determined from the Positive Matrix Factorization (PMF) analysis on the organic aerosol mass spectral matrix.

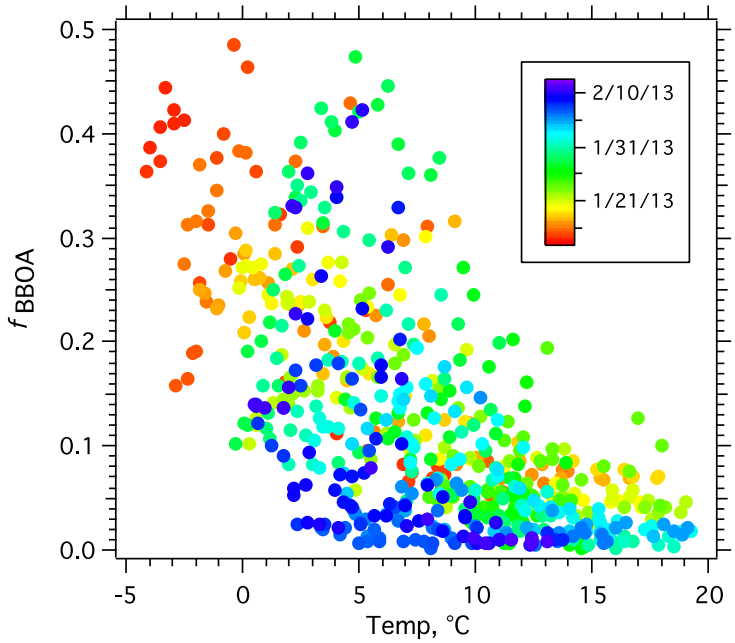

Figure S7. Correlation of the 1-hr average mass fraction of the AMS biomass burning organic aerosol component (f_{BBOA}) in the total PM_1 with the 1-hr average ambient temperature (Temp) during DISCOVER-AQ. The data are color-coded by the sampling date.

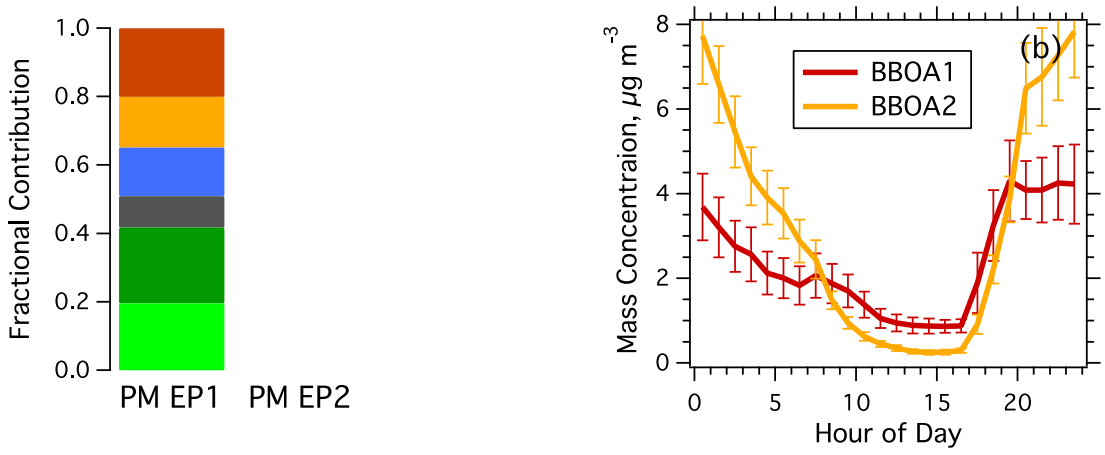

Figure S8. (a) Average fractional contribution of AMS organic aerosol (OA) factors, i.e., two types of biomass burning OA (BBOA-1 and BBOA-2), cooking OA (COA), hydrocarbon-like OA (HOA), low volatility oxygenated OA (LV-OOA) and semi-volatile oxygenated OA (SV-OOA), to total AMS OA mass for the two $PM_{2.5}$ episodes (1/14 – 1/23 and 1/29 – 2/5). (b) Diurnal plots of the mass concentrations of BBOA-1 and BBOA-2. The error bars are 1 sigma standard deviation of the diurnal averages.

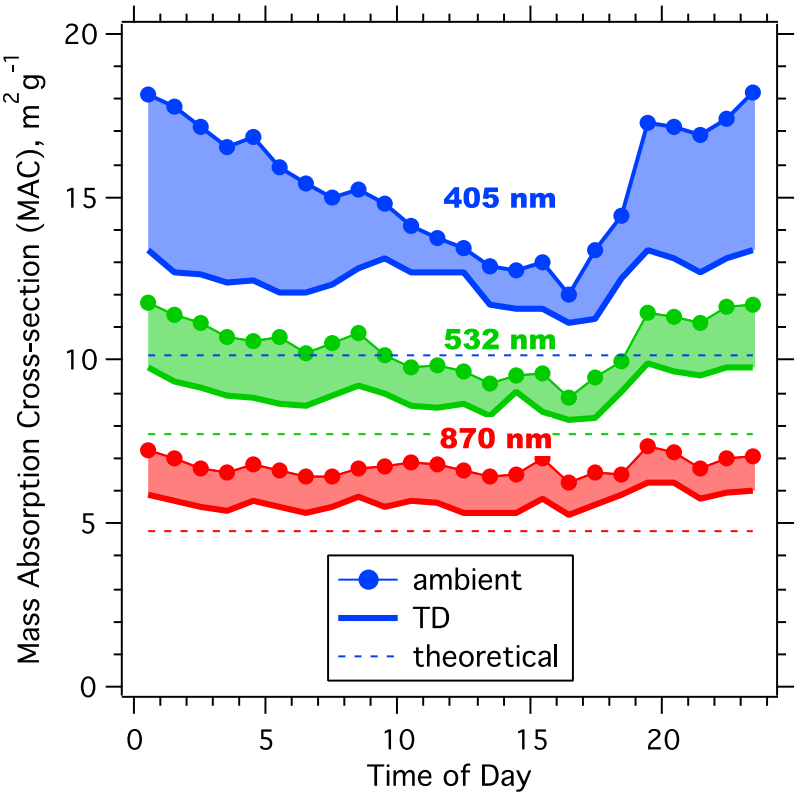

Figure S9. Diurnal profiles of the Mass Absorption Cross-section (*MAC*) of the ambient (lines with markers) and thermo-denuded (TD) (solid lines) $PM_{2.5}$ at 405, 532, and 870 nm. The dashed lines represent the *MAC* values recommended by *Bond and Bergstrom*[1] for freshly emitted black carbon particles at the corresponding wavelengths.

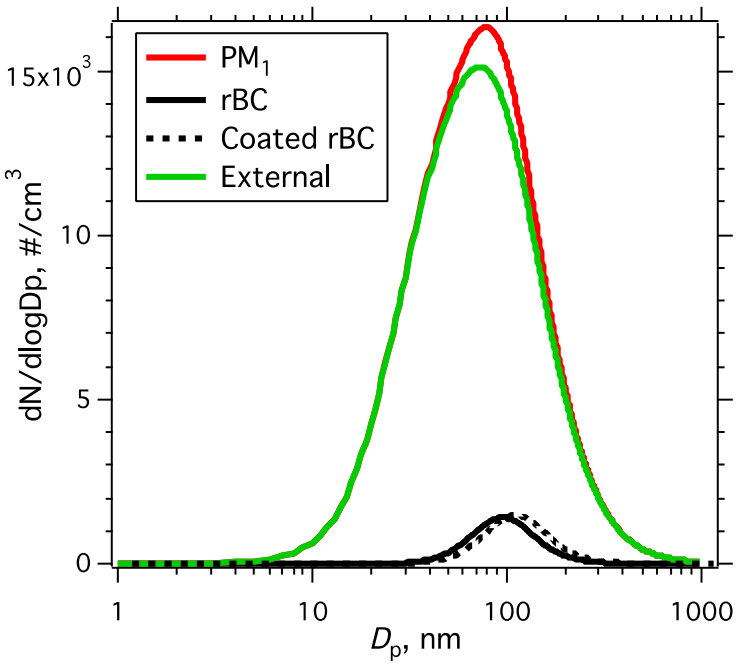

Figure S10. Campaign-average number-weighted size distributions ($dN/dlogD_p$) used as inputs to the Mie and RDG calculations. The refractory black carbon (rBC) size distribution was determined from the SP2 measurements, and the total PM_1 size distribution was determined from the SMPS measurements. The coated BC size distribution was constructed based on the estimated rBC equivalent coating thickness (or coating-to-core radius ratio, or r_{coat}/r_{core}). The externally mixed particle number size distribution ("External") was the difference between the total PM_1 and the coated BC number size distributions.

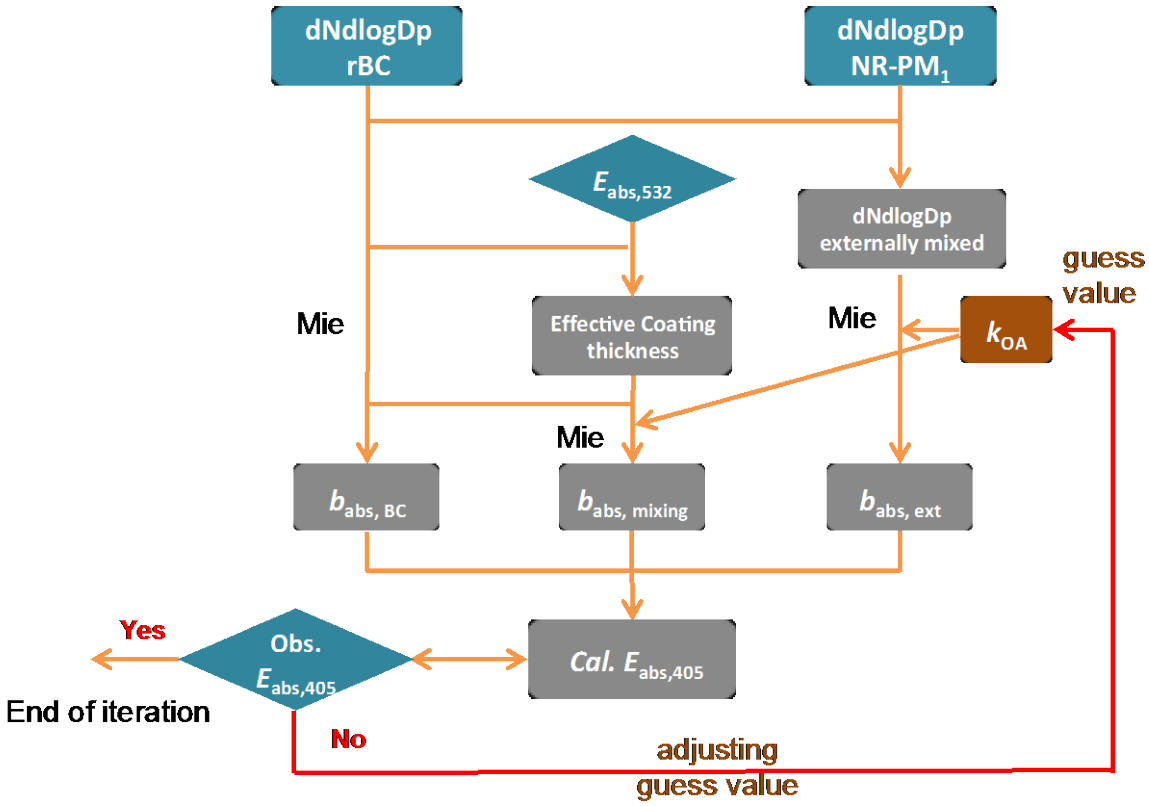

Figure S11. Schematic illustrating the retrieval process of the imaginary refractive index of the organic aerosols (k_{OA}) using optical closure analysis. The size distributions (dNdlogDp) of refractory black carbon (rBC) and non-refractory (NR) PM_1 were measured with a Single Particle Soot Photometer (SP2) and a Scanning Mobility Particle Sizer (SMPS), respectively. Observed absorption enhancement at 532 nm ($E_{abs,532}$) and 405 nm ($E_{abs,405}$) were determined with thermo-denuder (TD)-coupled absorption measurements using a Photo-Acoustic Spectrometer (PAS).

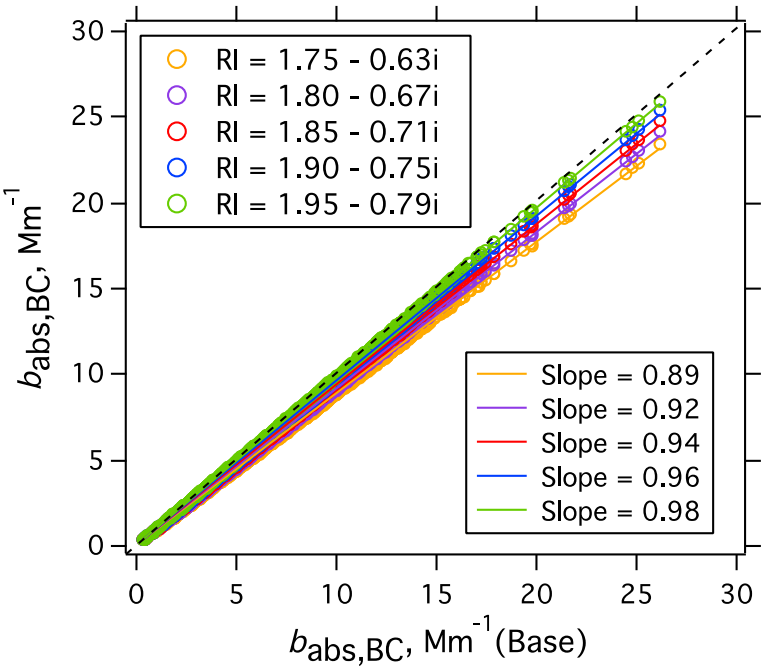

Figure S12. Sensitivity test on the calculated black carbon (BC) light absorption ($b_{abs,BC}$) at 532 nm using the base case Mie model with various refractive indices (RI) for BC as input. The RI values tested here are those listed in Table 5 and are from Bond and Bergstrom.[1] The base case RI (x-axis) is 1.88 -0.8*i*. The slopes are derived from the linear fits of $b_{abs,BC}$ calculated with the alternate RI values versus the base case.

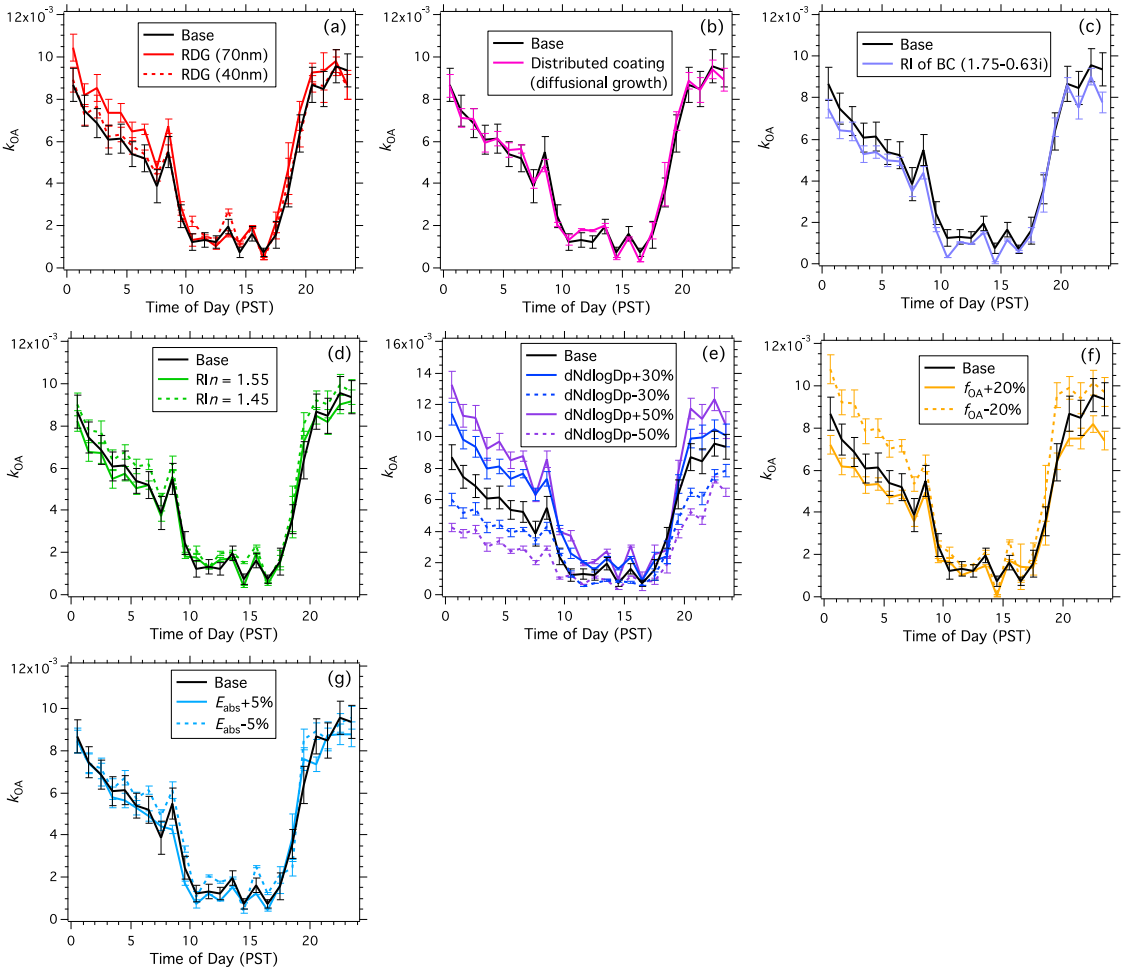

Figure S13. Diurnal plots of the refractive index of the organic component (k_{OA}) derived from the optical closure for the different sensitivity tests listed in Table 2. The result from the base case is shown as a solid black line in each panel and the results from the sensitivity tests as colored solid and dashed lines.

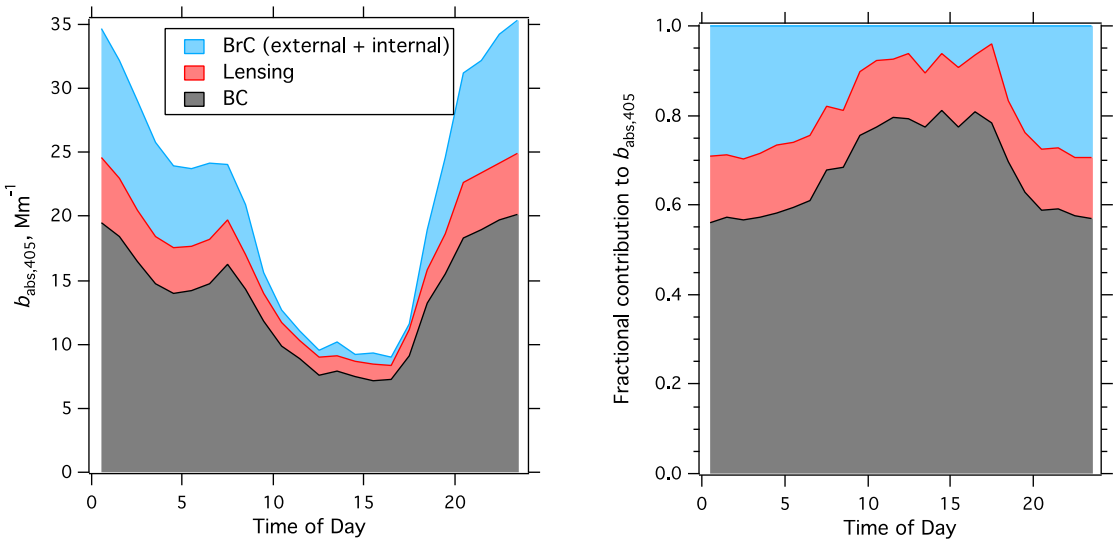

Figure S14. Apportionment of the $PM_{2.5}$ light absorption at 405 nm ($b_{abs,405}$): absolute values (left) and fractional contributions (right).